Euler Spiral for Shape Completion

BENJAMIN B. KIMIA, ILANA FRANKEL AND ANA-MARIA POPESCU
Division of Engineering, Brown University, Providence, R1 02912, USA

Abstract. In this paper we address the *curve completion* problem, e.g., the geometric continuation of boundaries of objects which are temporarily interrupted by occlusion. Also known as the gap completion or shape completion problem, this problem is a significant element of perceptual grouping of edge elements and has been approached by using cubic splines or biarcs which minimize total curvature squared (elastica), as motivated by a physical analogy. Our approach is motivated by railroad design methods of the early 1900's which connect two rail segments by "transition curves", and by the work of Knuth on mathematical typography. We propose that in using an energy minimizing solution completion curves should not penalize curvature as in elastica but curvature variation. The minimization of total curvature variation leads to an *Euler Spiral* solution, a curve whose curvature varies linearly with arclength. We reduce the construction of this curve from a pair of points and tangents at these points to solving a nonlinear system of equations involving Fresnel Integrals, whose solution relies on optimization from a suitable initial condition constrained to satisfy given boundary conditions. Since the choice of an appropriate initial curve is critical in this optimization, we analytically derive an optimal solution in the class of biarc curves, which is then used as the initial curve. The resulting interpolations yield intuitive interpolation across gaps and occlusions, and are extensible, in contrast to the scale-invariant version of elastica. In addition, Euler Spiral segments can be used in other applications of curve completions, e.g., modeling boundary segments between curvature extrema or modeling skeletal branch geometry.

1. Introduction

The human visual system is constantly confronted with complex scenes where objects are partially occluded by others, Fig. 1. Yet, it can effortlessly identify fragments which belong together and construct a complete object representation from them. Similar phenomena have been observed in completing the trajectory of a moving object which is temporarily occluded. Gestalt psychologists understood the significance of completing contours which are interrupted by occlusions and explored it, e.g., in the special case where the occluder blends with the background, thus generating *illusory or subjective contours*, Fig. 1. In computer vision, where results from low-level edge operators need to be grouped into complete object boundaries, e.g., for recognition, a number of approaches have been developed that take advantage of the properties of the completion contour to disambiguate the optimal grouping (Parent and Zucker, 1989; Sha'ashua and Ullman, 1988).

The process of completing contours beyond occlusions or across gaps, alternatively referred to as the *curve completion*, *gap completion*, or *shape completion* problem, is under-constrained: in completing a missing contour, e.g., the kangaroo's back across the occlusion in Fig. 1, there exist numerous curves that meet the "boundary conditions" of passing through specified endpoints and tangents. The selection of the optimal completion curve, therefore, has typically relied on assumptions regarding on what constitutes the most "likely" curve or the most "pleasing" or the "smoothest" curve (Nitzberg et al., 1993).

The explicit recovery of a completion curve is useful in a variety of visual tasks, such as the task of disambiguating edge maps in perceptual grouping, the partitioning of visual form for part-based

Figure 1. (a) Branches of a tree occlude each other, but each branch maintains its "identity" across such occlusions. (b) The same idea is illustrated for an occluded kangaroo where the continuity between the two separated segments is maintained. In addition, note that in mentally removing a part, e.g., the front paw, we are able to continue the main body outline. (c) Illusory contours arise from an occluder that blends with the background.

object representation and recognition, and for filling-in tasks in the reconstruction of occluded areas in figure-ground segregation. First, Fig. 2(a) depicts a series of edges which sample an object boundary, but with missing gaps and embedded in a set of spurious edges. In perceptual grouping tasks, spurious edges must be identified and removed, while gaps must be filled in. Williams and Thornber (1999) describe and compare a class of such approaches where an *affinity measure* is first computed for each pair of edges to describe the likelihood that they belong to the same boundary. This is then followed by an optimization over groupings of a larger set of edges, or curve hypotheses, to determine the saliency of each edge element. The properties of the completion curve, such as total curvature, have been used as the affinity measure, some of which require an explicit recovery of the completion curve. Second, the completion curve has been used as the "break curve" in partitioning shapes, where the properties of the completion curve are used to disambiguate conflicting part hypotheses, Fig. 2(b) (Dhandapani and Kimia, 2002; Siddiqi and Kimia, 1995). Third, in visual tasks emulating the filling-in

phenomenon and in inpainting, the presence of reconstructed contours allows for proper filling-in of the internal regions, thus avoiding diffusion in the missing contour areas, Fig. 2(c).

Curve Completion in Other Domains: The problem of selecting an optimal visual interpolation across missing boundaries is not unique to vision. In design, mechanical engineers have used "French Curves", a template consisting of a large number of smooth curves, to complete the partially specified surface of ships, aircraft fuselage, etc. (Farin, 1996), Fig. 3. Similarly, in computerized typography, where fonts need to be specified in a formal scalable language, partially specified letters and symbols need to be smoothly interpolated (Knuth, 1979). In compressing shapes for example, retaining a sampling of curvature extrema with their tangent is an efficient representation of the shape if appropriate contour completion algorithms are available. In civil engineering, this geometric interpolation problem arises in highway turn-out design, railroad construction, e.g., between two specified tunnel entrances, and the
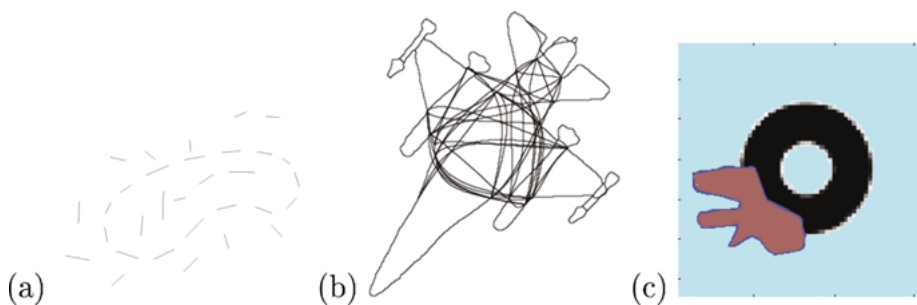

Figure 2. The Euler spiral completion curve is particularly useful in (a) disambiguating perceptual grouping of edge maps, (b) resolving conflicts among break curves in partitioning tasks, and (c) in augmenting the current inpainting techniques to avoid diffusion across missing boundaries.
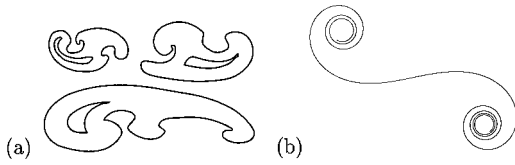
Figure 3. (a) The use of *French Curves* in the field of mechanical design employs was common place for drawing smooth curves of a range of curvatures (Weisstein, 1998). (b) We suggest here that segments of the Euler Spiral can serve this purpose well.

resulting curve is known as a *transition or easement curve* (Higgins, 1921; Kurtz, 1945; Talbot, 1927). More modern applications include the design of roller-coasters and bike tracks, Fig. 4. Finally in our own quotidian lives, we confront various forms of this problem, e.g., in parking and other driving scenarios.

In this paper, we assume that a pair of point-tangent pairs are under consideration, e.g., a candidate pair of T-junctions or curve endpoints. The properties of the optimal completion curve such as smoothness, length, etc. (Sha'ashua and Ullman, 1988) as well as its spatial interaction with existing curves and completion contours will be crucial in identifying the optimal grouping of point-tangent pairs. Thus, the problem we address can be formulated as:

Problem Statement: Given a pair of points $A_0(x_0, y_0)$ and $A_2(x_2, y_2)$, with associated unit tangent vectors, $\vec{T}_0(\cos\theta_0, \sin\theta_0)$ and $\vec{T}_2(\cos\theta_2, \sin\theta_2)$, find the most "pleasing" curve which passes through both points at their respective tangents.[1]

Despite the appeal of our visual intuition for the existence of a solution, this problem is under-specified

and has been the topic of numerous formalizations, especially in the context of subjective contours (Kanizsa, 1979). Ullman (1976) suggests that the interpolated curve $\mathcal{C}$, which should depend only on the relative geometry of the point-tangent pairs, must satisfy the following axioms:

1. $\mathcal{C}$ is invariant to rotations and translations (*isotropy*).
2. $\mathcal{C}$ is at least differentiable once (*smoothness*).
3. $\mathcal{C}$ minimizes total curvature—using the thin beam analogy (*minimum total curvature*).
4. $\mathcal{C}$ is *extensible* (originally referred to as locality); as defined below.

Definition. An interpolation $\mathcal{C}$ between $A_0(x_0, y_0, \theta_0)$[2] and $A_2(x_2, y_2, \theta_2)$ is *extensible* if for any $A_1(x_1, y_1, \theta_1)$ on $\mathcal{C}$ the interpolation between A_0 and A_1 and that between A_1 and A_2 both coincide with $\mathcal{C}$.

While Ullman hints at the doubly cantilever-ed beam and the related cubic spline approximation as the loci of minimum curvature (Ahlberg et al., 1967; Sokolnikoff, 1956), he proposes a completion curve consisting of two circular arcs, one tangent at one point edge and the other tangent to the other edge, and both tangent to each other. Since there exist multiple *biarc* solutions, the minimum total curvature property is used to select the optimal biarc. He then suggests a three-layer network with local connections to achieve this. As we shall see, the computation of a biarc solution is also integral to the approach here, but one which minimizes curvature difference not total curvature.

Rutkowski (1979) analyzes the minimum total curvature biarc construction of Ullman, describes a numerical method for computing it, and compares the results
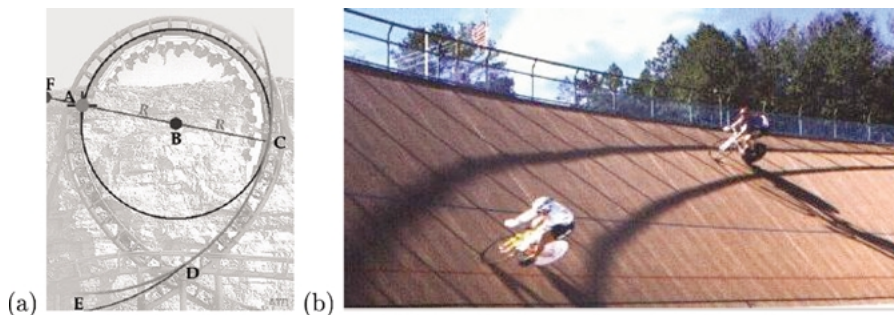

Figure 4. (a) In this Vekoma roller coaster, *Joker's Revenge*, the train runs backward; amusement-seekers leave the station with no view of where they are headed. In fact, they are about to loop a teardrop-shaped loop which is composed of a circular upper arc joined to lower *Euler Spiral* arcs (Baldwin, 1996). (b) The Velodrome at Stone Mountain Park, the Cycling Venue for the 1996 Olympic Games, is the first in a new generation of high-performance bike tracks these tracks are partially designed based on the Euler's spiral (http://www.kd3bj.ampr.org/track/).

to cubic polynomial completions. He concludes that "it appears that, in many cases, the cubic polynomial completions have a more pleasing appearance than the two circle completions." Brady and Grimson (1980) state that Ullman's biarc completion curve is, in fact, not extensible. They instead follow Knuth's approach (described below) of giving up on the extensibility axiom and support the use of cubic splines. Specifically, they propose to search in the space of cubic polynomial for the completion curve which minimizes a curve-related *energy*.

Consider the approach to the construction of a completion curve in typography where the shape of symbols is only partially specified by a collection of points, and needs to be completed in the most pleasing manner (Knuth, 1979). The fundamental problem underlying the mathematically rigorous design of these shapes—irrespective of style or size—can be posed as: "given a sequence of points in the plane, what is the most pleasing curve that connects them?" (Knuth, 1979). This problem, therefore, is similar (and later shown to be equivalent) to our geometric interpolation in that it requires the selection of an optimal curve which adheres to our traditional sense of aesthetic, axiomatizes the beauty of letters, and captures how "pleasing" the resulting interpolation is.[3] In light of this, and to allow for a certain degree of freedom in the interpolation, Knuth defines the most "pleasing" curve through a set of points $z_1, \ldots, z_n$, as the closed curve $\mathcal{C}$ which satisfies a set of axioms, somewhat similar to Ullman's axioms. Specifically, they require

1. $\mathcal{C}$ is invariant to translation, rotation, and scaling;
2. $\mathcal{C}$ is invariant to cyclic permutation or reversal of order of traversal (*symmetry*);
3. Adding a new point already on $\mathcal{C}$ to the list does not change this solution (*extensibility*);
4. $\mathcal{C}$ is locally constructed; i.e., each segment of the most pleasing curve between z_k and z_{k+1} depends only on (z_{k-1}, z_k, z_{k+1}, and z_{k+2}) (*locality*);
5. $\mathcal{C}$ has no sharp corners (*smoothness*); and,
6. If $\mathcal{C}$ interpolates four consecutive points lying on a circle, then C is a circle (*roundedness*).

Knuth then shows that these axioms in conjunction imply that: (i) the direction of the tangent to the most pleasing curve at z_k depends only on (z_{k-1}, z_k, z_{k+1}); (ii) this tangent must be tangent to the circle passing through (z_{k-1}, z_k, z_{k+1}); and, (iii) this tangent depends only on z_{k+1}, z_k, and the tangent at z_{k-1}. However, the latter implication violates the previous ones. Thus,

Knuth concludes that axioms 3, 4, 5, and 6 cannot be simultaneously satisfied, and remarks that although "the locality property is the most suspicious one," he does not want to give it up; hence he concludes that "the extensibility property has to go." The remaining axioms suggest a cubic spline interpolation for any interval (z_k, z_{k+1}) with known tangent-directions (computed from a local neighborhood based on the above conclusions) at these points—which is precisely the curve completion problem. Note, however, that the cubic spline interpolation does not satisfy axiom 6 since such an interpolation *can only approximate a circle*. Observe that due to the invariance axiom 1, we can generally state the final interpolation between any two point-tangent pairs as the cubic spline interpolation between $(0, 0, \theta_0)$ and $(1, 0, \theta_2)$ which is, in complex number notation:

$$z(s) = 3s^2 - 2s^3 + r_0 e^{i\theta_0} s(1-s)^2$$
$$- r_2 e^{i\theta_2} - s^2(1-s), \qquad (1)$$

where

$$r_0 = \max\left(\frac{1}{2}, \left|\frac{4\sin\theta_2}{\left(1 + \cos\left(\frac{\theta_0+\theta_2}{2}\right)\sin\left(\frac{\theta_0+\theta_2}{2}\right)\right)}\right|\right),$$

$$r_2 = \max\left(\frac{1}{2}, \left|\frac{4\sin\theta_0}{\left(1 + \cos\left(\frac{\theta_0+\theta_2}{2}\right)\sin\left(\frac{\theta_0+\theta_2}{2}\right)\right)}\right|\right).$$

The results of this interpolation, with and without the maximum operation specifying r_0 and r_2, are shown in Fig. 5. The application of this to type design gave rise to Knuth's METAFONT system which has been largely successful in the modern LaTeX computerized typesetting.[4]

Elastica: Horn argues that since the total energy stored in a thin beam (Horn, 1983) is proportional to the integral of the square of curvature, the curve which minimizes $\int \kappa^2 dS$ where κ is curvature and ds is arc-length, and which satisfies the given point-tangent boundary condition, represents the "smoothest" completion
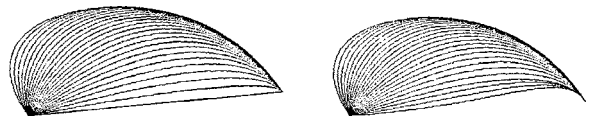

Figure 5. (a) The result of the interpolation without the maximum operation specifying r_0 and r_2 for a range of tangents. (b) The result of the interpolation with the maximum operation specifying r_0 and r_2, taken from Knuth (1979).

shape. He derives differential equations for this curve both in terms of elliptic integrals and Cartesian coordinates. It is then shown that this completion curve is extensible. In relation to minimum total curvature biarcs of Ullman (1976), he also examines the optimal multi-arc approximations, and observes that in this multi-arc solution arcs tend to be of equal length while curvature increases more or less linearly along the curve. Interestingly, this property implicitly points to the Euler Spiral presented here; however, he finds that the latter curve has higher total squared curvature than the multi-arc solution with a sufficient number of segments. Thus, the Euler Spiral is not seen to be an appropriate candidate for shape completion.[5]

More recently, Mumford (1994) notes the historical role of *elastica* in obtaining the *optimal* curve through two specified points with specified orientations (Euler, 1744; Love, 1927; Bryant and Griffiths, 1986), i.e., the curve which minimizes

$$\int (\alpha \kappa^2 + \beta) \, ds, \qquad (2)$$

where α, β are constants. Mumford interprets these elastica from the Bayesian view as "the mode of the probability distribution underlying a certain stochastic process restricted to curves with prescribed boundary behavior" (Mumford, 1994), Fig. 6. Similarly, Williams and Jacobs (1995, 1997) model the completion shapes as the most likely one in a family of curves, and like Mumford, model this by a random walk in the space of positions and orientations, leading to a *stochastic completion field.* An extensive model has been developed on this idea for disambiguation of edge maps and perceptual grouping (Williams and Jacobs, 1995, 1997; Williams and Thornber, 1998).

The major shortcomings of the elastica are that (i) they are not scale-invariant, (ii) they are computationally expensive to derive, and (iii) they do not lead to circular completion curves when the point-tangent pairs are, in fact, co-circular (i.e., both lie on the same circle). Scale-invariance is necessary since these curves are used to model completion say gap completion, in a world where the distance from the observer to the imaged object varies constantly, yet the gaps must be
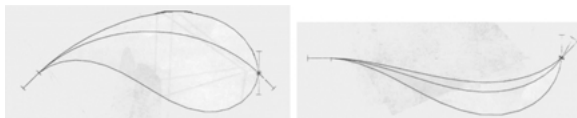

Figure 6.   Examples of elastica from Mumford (1994).

completed consistently. Even when $\beta = 0$, the energy of the curve, and thus its "salience", varies with scale (distance between points) relative to competing hypotheses. This has prompted an approach wherein the elastica energy is scaled by total length (Sharon et al., 2000; Weiss, 1988; Onn and Bruckstein, 1990). But this implies that the computation of the completion curve becomes global, and thus is not *extensible*: given any point on a completion curve $\mathcal{C}$, the two completion sub-problems do not necessarily coincide with the same $\mathcal{C}$.

Sharon et al. (2000) address the computational aspects of finding the optimal completion curve and propose analytic expressions for approximating it. Based on the assumption that the deviation angle of the tangents from the line connecting the endpoints is small, they derive cubic Hermite spline approximations. A second expression in terms of these deviation angles is then shown to be accurate even when the above assumption is not valid. The result is a numerical method which is accurate and relatively fast.

We now motivate a new approach by first considering the third difficulty, namely, that elastica, least energy curves minimizing $\int \kappa^2$, do not lead to circular interpolations (Sharon et al., 2000). The intuition that two (co-circular (Parent and Zucker, 1989)) edge elements with equal angles to the line connecting them should be completed via a circular arc *regardless of curvature* thus argues for minimizing not total curvature but total *change in curvature*. We propose that the energy functional which properly captures the elusive nature of "the most pleasing curve" penalizes *change in curvature*, but not necessarily curvature proper. Thus, we seek the curve specified with the curvature function $\kappa(s)$, $s \in [0, L]$ and with arc-length L which minimizes

$$E[\kappa] = \int_0^L \kappa_s^2 \, ds, \qquad (3)$$

subject to the boundary conditions $(x_0, \ y_0, \ \theta_0)$, (x_2, y_2, θ_2). Using calculus of variation the corresponding Euler-Lagrange equation is $\kappa_{ss} = 0$, for which the general solution is the linear curvature curve $\kappa(s) = \gamma s + \kappa_0$, with two arbitrary parameters κ_0 and γ. However, we have yet to satisfy the boundary constraints in this optimization. Observe that in the case of elastica the unconstrained Euler-Lagrange equation for $\int \kappa^2 \, ds$ leads to $\kappa = 0$, which generally cannot satisfy endpoint constraints.[6] In our case, these endpoint constraints *can* be satisfied for the general class of curves described by

$\kappa_{ss} = 0$—that is, the class of curves described by linear curvature profiles, otherwise known, in the mathematical literature, as the *Euler Spiral*, the *Cornu Spiral* or the *clothoids*, and, in civil engineering, as the *Railroad Spiral* or the *Transition Curve*.

The paper is organized as follows. In Section 2 we will examine equations for the construction of the Euler spiral and identify parameters needed to specify it in a form that is suitable for this problem. In Section 3, we will address the question of finding parameters such that the Euler Spiral segment meets the end-points with specified tangents, thus solving the curve completion problem. We reduce this to solving a system of non-linear equations in two unknowns which we then solve by numerical optimization from a closeby initial curve estimate. We rely on a *biarc* initial estimate which minimizes total squared curvature change, as opposed to Ullman's biarc which minimizes total curvature squared. Towards this end, Section 4 examines the space of biarcs which meet the end-points at specified tangents and analytically derives the optimal biarc in the sense of the minimal curvature change. This biarc, with a piecewise constant curvature profile, is in fact geometrically close to the Euler spiral which has a linear curvature profile and is used as the initial estimate to derive the optimization. Section 5 presents examples of the Euler spiral interpolation for synthetic and realistic solutions, which are intuitive and extensible.

2. Euler's Spiral

The Euler Spiral was considered by Euler in connection to his investigation of a freely coiled up elastic spring held taut horizontally by a weight at its extremity (Euler, 1744). In its natural, relaxed position, the spring satisfies $\kappa = \frac{1}{a^2}s$, where a is a constant, s is arc-length, and κ is curvature. By a simple integration of curvature and then the tangent angle $\theta(s)$ we obtain the equations for the curve $\mathcal{C}(s) = (x(s), y(s))$,

$$\theta(s) = \frac{s^2}{2a^2}, \quad \mathcal{C}(s) = \int_0^s e^{\frac{i\xi^2}{2a^2}} d\xi. \tag{4}$$

This set of integrals came to be known as the Fresnel's (1788–1827) integrals in connection with his model of

the intensity of the illumination of a diffraction pattern as the sum of squares of each such integral (Euler's, 1918), $C^2(s) + S^2(s)$, where C and S are the Fresnel Integral,

$$(C(s), S(s))$$
$$:= \left(\int_0^s \cos\left(\frac{\pi}{2}\xi^2\right) d\xi, \quad \int_0^s \sin\left(\frac{\pi}{2}\xi^2\right) d\xi \right),$$
$$F(s) = C(s) + i S(s), \tag{5}$$

which are typically either calculated and readily available from tables originally created by Fresnel, expanded in terms of the spherical Bessel Functions (Abramowitz and Stegun, 1972; Leonard, 1988; Press et al., 1993; Spanier and Oldham, 1987), or computed by integrating the Taylor expansion term by term (Abramowitz and Stegun, 1972; Press et al., 1993):

$$C(s) = \sum_{n=0}^{\infty} \frac{(-1)^n \left(\frac{\pi}{2}\right)^{2n}}{(2n)!(4n+1)} s^{4n+1},$$

$$S(s) = \sum_{n=0}^{\infty} \frac{(-1)^n \left(\frac{\pi}{2}\right)^{2n+1}}{(2n+1)!(4n+3)} s^{4n+3}.$$

Then, in 1874, Cornu plotted the Euler's Spiral accurately (Cornu, 1874); the curve thus acquired another name: Cornu's Spiral. And Cesaro, upon studying the curve and establishing a number of its properties, dubbed it the "clothoid" from the Greek word meaning "to twist by spinning" (Cesaro, 1886). Note that we henceforth refer to this curve as the Euler's Spiral in connection with Euler's investigations of it.

It is immediately apparent that the computation and visualization of the Euler Spiral relies on the Fresnel integrals. The following proposition states the general form of the Euler spiral with a specified boundary condition.

Proposition 1. *The general form of the Euler Spiral* $\mathcal{C}(s)$, *which passes through* $\mathcal{C}_0(x_0, y_0)$ *at tangent angle* θ_0, *with curvature* κ_0, *and a rate of change of curvature*

γ, *can be written as*

$$\begin{cases} \mathcal{C}_0 + e^{i\theta_0}s & \gamma = 0, \kappa_0 = 0 \\ \mathcal{C}_0 + \dfrac{e^{i\theta_0}}{\kappa_0}(\sin(\kappa_0 s) + i(1 - \cos(\kappa_0 s))) & \gamma = 0, \kappa_0 \neq 0 \\ \mathcal{C}_0 + \sqrt{\dfrac{\pi}{|\gamma|}}e^{i\left(\theta_0 - \frac{\kappa_0^2}{2\gamma}\right)} \times \left[sign(\gamma)\left(C\left(\dfrac{\kappa_0 + \gamma s}{\sqrt{\pi|\gamma|}}\right) - C\left(\dfrac{\kappa_0}{\sqrt{\pi|\gamma|}}\right)\right) + i\left(S\left(\dfrac{\kappa_0 + \gamma s}{\sqrt{\pi|\gamma|}}\right) - S\left(\dfrac{\kappa_0}{\sqrt{\pi|\gamma|}}\right)\right)\right], & \gamma \neq 0 \end{cases}$$

$$(6)$$

and $\theta(s) = \frac{1}{2}\gamma s^2 + \kappa_0 s + \theta_0$ in all cases.

Proof: The Euler spiral $\mathcal{C}(s)$ is obtained by integrating $\kappa(s) = \gamma s + \kappa_0$ using Eq. (4), giving

$$\begin{cases} \theta(s) = \dfrac{1}{2}\gamma s^2 + \kappa_0 s + \theta_0, \\ \mathcal{C}(s) = \mathcal{C}_0 + \displaystyle\int_0^s e^{i\left(\frac{1}{2}\gamma\xi^2 + \kappa_0\xi + \theta_0\right)} d\xi. \end{cases} \quad (7)$$

First, if $\gamma = 0$ and $\kappa_0 = 0$, it is straightforward to derive the first expression in Eq. (6), which gives a straight line. Second, if $\gamma = 0$ and $\kappa_0 \neq 0$, then

$$\begin{aligned} \mathcal{C}(s) &= \mathcal{C}_0 + e^{i\theta_0}\int_0^s e^{i\kappa_0\xi} d\xi \\ &= \mathcal{C}_0 + i\frac{e^{i\theta_0}}{\kappa_0}(1 - e^{i\kappa_0 s}), \quad (8) \end{aligned}$$

leading to the second expression in Eq. (6), which gives a circle. Finally, when $\gamma \neq 0$, consider first $\gamma > 0$. We complete the square term in the exponent in Eq. (7) and using the substitution $\sqrt{\frac{\gamma}{2}}\xi + \sqrt{\frac{2}{\gamma}}\frac{\kappa_0}{2} = \sqrt{\frac{\pi}{2}}\tau$, obtain

$$\mathcal{C}(s) = \mathcal{C}_0 + \int_0^s e^{i\left(\left(\sqrt{\frac{\gamma}{2}}\xi + \sqrt{\frac{2}{\gamma}}\frac{\kappa_0}{2}\right)^2 + \theta_0 - \frac{\kappa_0^2}{2\gamma}\right)} d\xi, \quad (9)$$

$$= \mathcal{C}_0 + e^{i\left(\theta_0 - \frac{\kappa_0^2}{2\gamma}\right)}\sqrt{\frac{\pi}{2}}\int_{\frac{\kappa_0}{\sqrt{\pi\gamma}}}^{\frac{(\kappa_0 + \gamma s)}{\sqrt{\pi\gamma}}} e^{i\frac{\pi\tau^2}{2}} d\tau. \quad (10)$$

which gives,

$$\begin{aligned} \mathcal{C}(s) = \mathcal{C}_0 + &\sqrt{\frac{\pi}{\gamma}}e^{i\left(\theta_0 - \frac{\kappa_0^2}{2\gamma}\right)}\left[\left(C\left(\frac{\kappa_0 + \gamma s}{\sqrt{\pi\gamma}}\right)\right.\right. \\ &- C\left(\frac{\kappa_0}{\sqrt{\pi\gamma}}\right)\right) + i\left(S\left(\frac{\kappa_0 + \gamma s}{\sqrt{\pi\gamma}}\right)\right. \\ &\left.\left. - S\left(\frac{\kappa_0}{\sqrt{\pi\gamma}}\right)\right)\right]. \quad (11) \end{aligned}$$

For $\gamma < 0$, the computations are similar, except that $\sqrt{-\gamma}$ is used instead, leading to the term in Eq. (6). $\square$

Thus, given (x_0, y_0, θ_0), two free parameters κ_0 and γ must be obtained in order to define the spiral. An additional parameter L is needed to delineate a segment of the spiral by its total length; so *six* parameters in total, (x_0, y_0, θ_0) and (κ_0, γ, L), are required in order to define an *Euler Spiral segment*, the canonical geometrical element which we later use to solve the curve completion problem. The spirals in Fig. 7 illustrate the effect of varying κ_0 and γ for fixed L.

3. Euler's Spiral for Curve Completion

We now examine how the Euler Spiral segment can be used for the geometric interpolation of two point-tangent pairs for curve completion.

Proposition 2. *Consider the Euler Spiral $\mathcal{C}(s)$ satisfying end-point conditions $\mathcal{C}_0(x_0, y_0)$ with*
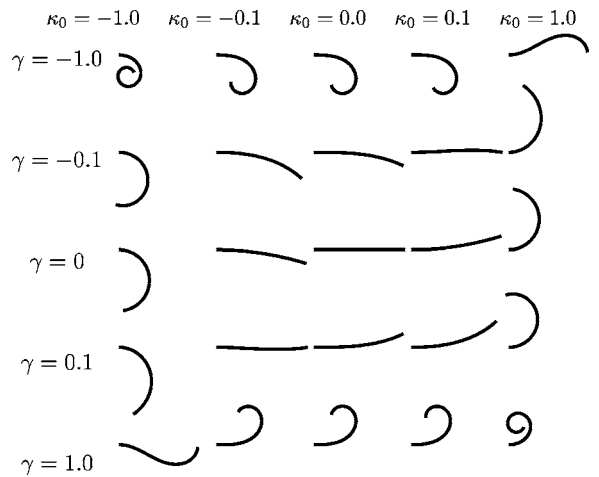

Figure 7. An Euler spiral segment starting at the origin and tangent to the x-axis of a given length is shown by varying initial curvature κ_0 and rate of change of curvature γ of the Euler Spiral.

tangent $\vec{T}_0(\cos\theta_0, \sin\theta_0)$, and $\mathcal{C}_2(x_2, y_2)$ with tangent $\vec{T}_2(\cos\theta_2, \sin\theta_2)$, which is identified by six parameters $(x_0, y_0, \theta_0, \kappa_0, \gamma, L)$. Let $\mathcal{C}_2 - \mathcal{C}_0 = L_0 e^{i\psi}$. Then, if the point-tangent pairs are cocircular, i.e., if $\psi = \frac{\theta_2 + \theta_0}{2}$, then $\gamma = 0$, $\kappa_0 = \kappa_2 = \frac{2}{L_0}\sin(\frac{\theta_0 - \theta_2}{2})$ and $L = \frac{L_0(\theta_0 + \theta_2)}{4\sin(\frac{\theta_0 + \theta_2}{2})}$. Otherwise, if $\psi \neq \frac{\theta_2 + \theta_0}{2}$, then

$$\begin{cases} \gamma = \dfrac{\kappa_2^2 - \kappa_0^2}{2(\theta_2 - \theta_0)}, \\ L = \dfrac{2(\theta_2 - \theta_0)}{\kappa_2 + \kappa_0}, \end{cases} \tag{12}$$

where κ_0 and κ_2 satisfy

$$\begin{aligned} \mathcal{C}_2 &- \mathcal{C}_0 \\ &= \sqrt{2\pi}\sqrt{\left|\frac{\theta_2 - \theta_0}{\kappa_2^2 - \kappa_0^2}\right|} e^{i\left(\frac{\theta_0\kappa_2^2 - \theta_2\kappa_0^2}{\kappa_2^2 - \kappa_0^2}\right)} \\ &\times \left[sign\left(\frac{\kappa_2^2 - \kappa_0^2}{\theta_2 - \theta_0}\right)\left[C\left(\sqrt{\frac{2}{\pi}}\sqrt{\left|\frac{\theta_2 - \theta_0}{\kappa_2^2 - \kappa_0^2}\right|}\kappa_2\right)\right.\right. \\ &\left.- C\left(\sqrt{\frac{2}{\pi}}\sqrt{\left|\frac{\theta_2 - \theta_0}{\kappa_2^2 - \kappa_0^2}\right|}\kappa_0\right)\right] \\ &+ i\left[S\left(\sqrt{\frac{2}{\pi}}\sqrt{\left|\frac{\theta_2 - \theta_0}{\kappa_2^2 - \kappa_0^2}\right|}\kappa_2\right)\right. \\ &\left.\left.- S\left(\sqrt{\frac{2}{\pi}}\sqrt{\left|\frac{\theta_2 - \theta_0}{\kappa_2^2 - \kappa_0^2}\right|}\kappa_0\right)\right]\right] \end{aligned}$$

Proof: Observe that the input is specified through six known variables $(x_0, y_0, \theta_0; x_2, y_2, \theta_2)$. The description of the Euler Spiral also requires six parameters, $(x_0, y_0, \theta_0; \kappa_0, \gamma, L)$, which explicitly include parameters defining $\mathcal{C}_0$ and $\vec{T}_0$, namely, (x_0, y_0, θ_0). Thus, we need to compute (κ_0, γ, L) such that the spiral segment ends at $\mathcal{C}_2$ with tangent $\vec{T}_2$. This gives two constraints,

$$\begin{cases} C(L) = \mathcal{C}_2, \\ \theta(L) = \theta_2, \end{cases} \tag{13}$$

where C and θ are specified in Proposition 1. This gives three equations for the three unknowns (κ_0, γ, L), in terms of the known parameters $(x_0, y_0, \theta_0; x_2, y_2, \theta_2)$. Note that the equation for θ_2 can be used effectively to reduce the parameter search by one.[7] Consider κ_0 and κ_2, the curvatures at $\mathcal{C}_0$ and $\mathcal{C}_2$, respectively, as a set of free parameter, i.e., κ_2 rewrite γ, L in terms of κ_0

and κ_2.

$$\begin{cases} \kappa_2 = \gamma L + \kappa_0, \\ \theta_2 = \dfrac{1}{2}\gamma L^2 + \kappa_0 L + \theta_0, \end{cases} \tag{14}$$

and simplifying $\theta_2 = \frac{1}{2}(\kappa_2 - \kappa_0)L + \kappa_0 L + \theta_0 = \frac{\kappa_2 + \kappa_0}{2}L + \theta_0$, results in Eq. (12) for L. In other words, the length of a spiral segment is the change in orientation $(\theta_2 - \theta_0)$ divided by its average curvature $(\frac{\kappa_2 + \kappa_0}{2})$. In addition, note that if $\kappa_0 \neq \kappa_2$ we derive expressions

$$\begin{aligned} \sqrt{\frac{\pi}{|\gamma|}} &= \sqrt{2\pi}\sqrt{\left|\frac{\theta_2 - \theta_0}{\kappa_2^2 - \kappa_0^2}\right|}, \\ \theta_0 - \frac{\kappa_0^2}{2\gamma} &= \theta_0 - \kappa_0^2\left(\frac{\theta_2 - \theta_0}{\kappa_2^2 - \kappa_0^2}\right) \\ &= \frac{\theta_0\kappa_2^2 - \theta_2\kappa_0^2}{\kappa_2^2 - \kappa_0^2}, \\ \frac{\kappa_0 + \gamma L}{\sqrt{\pi|\gamma|}} &= \kappa_2\sqrt{\frac{2}{\pi}}\sqrt{\left|\frac{\theta_2 - \theta_0}{\kappa_2^2 - \kappa_0^2}\right|}, \end{aligned} \tag{15}$$

which are needed to simplify Eq. (13) in terms of two unknowns (κ_0, κ_2). If $\psi = \frac{\theta_0 + \theta_2}{2}$, the two point-tangent pairs are cocircular. with $\kappa_0 = \kappa_2 = \frac{2}{L_0}\sin\frac{\theta_0 + \theta_2}{2}$, $L = \frac{L_0(\theta_0 + \theta_2)}{4\sin(\frac{\theta_0 + \theta_2}{2})}$. Obviously, a circular arc is an Euler Spiral segment with $\gamma = 0$, so that it solves the geometric interpolation problem. On the other hand, if $\psi \neq \frac{\theta_0 + \theta_2}{2}$, then $\kappa_0 \neq \kappa_2$, $\gamma \neq 0$, and we have

$$\begin{aligned} \mathcal{C}_2 &= \mathcal{C}_0 + \sqrt{\frac{\pi}{|\gamma|}} e^{i\left(\theta_0 - \frac{\kappa_0^2}{2\gamma}\right)} \left[sign(\gamma)\left[C\left(\frac{\kappa_0 + \gamma L}{\sqrt{\pi|\gamma|}}\right)\right.\right. \\ &\left.- C\left(\frac{\kappa_0}{\sqrt{\pi|\gamma|}}\right)\right] + i\left[S\left(\frac{\kappa_0 + \gamma L}{\sqrt{\pi|\gamma|}}\right)\right. \\ &\left.\left.- S\left(\frac{\kappa_0}{\sqrt{\pi|\gamma|}}\right)\right]\right] \\ &= \mathcal{C}_0 + \sqrt{2\pi}\sqrt{\left|\frac{\theta_2 - \theta_0}{\kappa_2^2 - \kappa_0^2}\right|} e^{i\left(\frac{\theta_0\kappa_2^2 - \theta_2\kappa_0^2}{\kappa_2^2 - \kappa_0^2}\right)} \\ &\times \left[sign\left(\frac{\kappa_2^2 - \kappa_0^2}{\theta_2 - \theta_0}\right)\left[C\left(\sqrt{\frac{2}{\pi}}\sqrt{\left|\frac{\theta_2 - \theta_0}{\kappa_2^2 - \kappa_0^2}\right|}\kappa_2\right)\right.\right. \\ &\left.\left.- C\left(\sqrt{\frac{2}{\pi}}\sqrt{\left|\frac{\theta_2 - \theta_0}{\kappa_2^2 - \kappa_0^2}\right|}\kappa_0\right)\right]\right. \end{aligned}$$
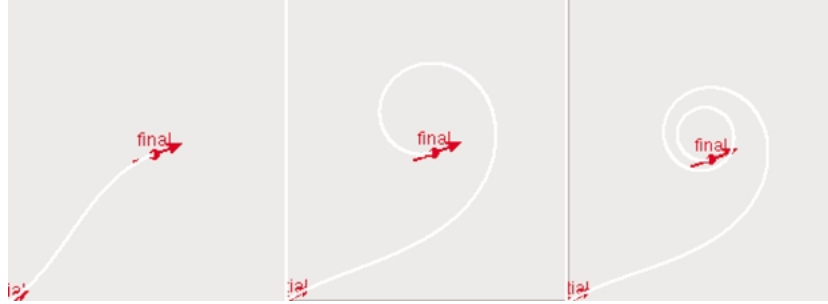
Figure 8. Given a pair of points-tangent pairs specified by, $(x_0, y_0, \theta_0; x_2, y_2, \theta_2)$, multiple solutions can be obtained as the Euler Spiral can reach the same angle infinitely many times due to its winding nature, as illustrated above. We seek the shortest solution which do not wind more than 2π.

$$+ i \left[S\left(\sqrt{\frac{2}{\pi}} \sqrt{\left| \frac{\theta_2 - \theta_0}{\kappa_2^2 - \kappa_0^2} \right|} \kappa_2 \right) \right.$$
$$\left. - S\left(\sqrt{\frac{2}{\pi}} \sqrt{\left| \frac{\theta_2 - \theta_0}{\kappa_2^2 - \kappa_0^2} \right|} \kappa_0 \right) \right] \right], \tag{16}$$

a system of two equations in two unknowns (κ_0, κ_2). $\quad \square$

Since there is no known direct analytic solution for this nonlinear set of equations, we employ numerical optimization, i.e., a gradient descent approach, starting from a suitable initial estimate, such that the initial estimate is *evolved* until the final Euler spiral solution is reached. Due to its spiral nature, the Euler Spiral reaches the same angle infinitely many times, Fig. 8. We are, however, only interested in the *shortest* solution—thus the overall range of $\theta(s)$ is restricted to 2π. In consideration of this constraint, the selection of an appropriate initial estimate (the biarc approximation) and the use of explicit constraints in the numerical optimization become critical, as discussed in Section 4. We first show that the Euler spiral has the required properties of visual interpolation for shape completion.

Proposition 3. *The Euler Spiral ES passing through (x_0, y_0, θ_0) and (x_2, y_2, θ_2) satisfies the visual interpolation's required property of invariance to translation, rotation and scaling. That is, the ES interpolations of translated, rotated, scaled boundary conditions data is the translation, rotation, or scaling of the ES interpolation of the initial boundary conditions.*

Proof: The proof for translation and rotation is trivial since Eq. (13) contains relative terms $\mathcal{C}_2 - \mathcal{C}_0$ and

$\theta_2 - \theta_0$. To show scale invariance, we have to show that parameters pertaining to a scaled Euler Spiral satisfy Eq. (13) for scaled parameters. A scaling by a factor of α scales $\mathcal{C}_2 - \mathcal{C}_0$ by this factor, but does not affect $\theta_2 - \theta_0$. A scaling of the Euler Spiral, on the other hand, scales its curvature by $\frac{1}{\alpha}$ and its rate of change of curvature by $\frac{1}{\alpha^2}$. Thus, it must be shown that $\tilde{\kappa}_0 = \frac{\kappa_0}{\alpha}$, $\tilde{\kappa}_2 = \frac{\kappa_2}{\alpha}$, and $\tilde{\gamma} = \frac{1}{\alpha^2}\gamma$ satisfy Eq. (13) for $\alpha(\mathcal{C}_2 - \mathcal{C}_0)$, i.e., that the right hand side is scaled by α, which is evident by a term by term examination. $\quad \square$

Proposition 4. *The Euler Spiral interpolation between $\mathcal{C}_0(x_0, y_0, \theta_0)$ and $\mathcal{C}(x_2, y_2, \theta_2)$ is extensible.*

Proof: The proof is rather straightforward. Let $C_1(x_1, y_1, \theta_1)$ be an arbitrary point on the Euler Spiral interpolation between $\mathcal{C}_0(x_0, y_0, \theta_0)$ and $\mathcal{C}_2(x_2, y_2, \theta_2)$, specified by $(x_0, y_0, \theta_0, \kappa_0, \kappa_2, \gamma)$ as defined in Proposition 3, where θ_i is the tangent of the Euler spiral at (x_i, y_i). Let L_1 and κ_1 be the length parameter and curvature of the Euler Spiral at $\mathcal{C}_1$, respectively. Since $\mathcal{C}_1(x_1, y_1, \theta_1)$ is a point of the interpolation, we have

$$\begin{cases} \mathcal{C}_1 = \mathcal{C}_0 + \sqrt{\frac{\pi}{|\gamma|}} e^{i\left(\theta_0 - \frac{\kappa_0^2}{2\gamma}\right)} \left[sign(\gamma) \left(\mathcal{C}\left(\frac{\kappa_0 + \gamma L_1}{\sqrt{\pi|\gamma|}} \right) \right. \right. \\ \quad \left. - \mathcal{C}\left(\frac{\kappa_0}{\sqrt{\pi|\gamma|}} \right) \right) + i \left(S\left(\frac{\kappa_0 + \gamma L_1}{\sqrt{\pi|\gamma|}} \right) \right. \\ \quad \left. \left. - S\left(\frac{\kappa_0}{\sqrt{\pi|\gamma|}} \right) \right) \right] \\ \theta_1 = \frac{1}{2}\gamma L_1^2 + \kappa_0 L_1 + \theta_0, \end{cases} \tag{17}$$

where $\kappa_1 = \kappa_0 + \gamma L_1$. We now seek the interpolation between $\mathcal{C}_1$ and $\mathcal{C}_2$ as the solution $(\tilde{\kappa}_0, \tilde{\gamma}, \tilde{L})$ of

$$
\begin{cases}
\mathcal{C}_2 = \mathcal{C}_1 + \sqrt{\dfrac{\pi}{|\tilde{\gamma}|}} e^{i\left(\tilde{\theta}_0 - \frac{\tilde{\kappa}_0^2}{2\tilde{\gamma}}\right)} \left[sign(\tilde{\gamma}) \left(C\left(\dfrac{\tilde{\kappa}_0 + \tilde{\gamma}\tilde{L}}{\sqrt{\pi|\tilde{\gamma}|}}\right) \right. \right. \\
\qquad \left. - C\left(\dfrac{\tilde{\kappa}_0}{\sqrt{\pi|\tilde{\gamma}|}}\right) \right) + i \left(S\left(\dfrac{\tilde{\kappa}_0 + \tilde{\gamma}\tilde{L}}{\sqrt{\pi|\tilde{\gamma}|}}\right) \right. \\
\qquad \left. \left. - S\left(\dfrac{\tilde{\kappa}_0}{\sqrt{\pi|\tilde{\gamma}|}}\right) \right) \right] \\
\theta_2 = \dfrac{1}{2}\tilde{\gamma}\tilde{L}^2 + \tilde{\kappa}_0\tilde{L} + \theta_1.
\end{cases} \tag{18}
$$

We need to show that the previous Euler spiral is the solution here, i.e., the Euler spiral with $\tilde{\gamma} = \gamma$, $\tilde{\kappa}_0 = \kappa_1 = \kappa_0 + \gamma L_1$ and $\tilde{L} = L - L_1$ solves the above equations. In this case, the right hand side of the second equation in (18) is

$$
\frac{1}{2}\tilde{\gamma}\tilde{L}^2 + \tilde{\kappa}_0\tilde{L} + \theta_1
$$
$$
= \frac{1}{2}\gamma(L - L_1)^2 + \kappa_1(L - L_1) + \theta_1, \quad (19)
$$

which after expanding the first two terms and simplifying the resulting expression, yields θ_2. Similarly, we show the correctness of the first equation in (18) by simplifying the right hand side

$$
\text{RHS} = \mathcal{C}_1 + \sqrt{\frac{\pi}{|\gamma|}} e^{i\left(\frac{1}{2}\gamma L_1^2 + \kappa_0 L_1 + \theta_0 - \frac{(\kappa_0 + \gamma L_1)^2}{2\gamma}\right)}
$$
$$
\times \left[sign(\gamma) \left(C\left(\frac{\kappa_0 + \gamma L_1 + \gamma(L - L_1)}{\sqrt{\pi|\gamma|}}\right) \right. \right.
$$
$$
\left. - C\left(\frac{\kappa_0 + \gamma L_1}{\sqrt{\pi|\gamma|}}\right) \right)
$$
$$
+ i \left(S\left(\frac{\kappa_0 + \gamma L_1 + \gamma(L - L_1)}{\sqrt{\pi|\gamma|}}\right) \right.
$$
$$
\left. \left. - S\left(\frac{\kappa_0 + \gamma L_1}{\sqrt{\pi|\gamma|}}\right) \right) \right]
$$
$$
= \mathcal{C}_1 + \sqrt{\frac{\pi}{|\gamma|}} e^{i\left(\theta_0 - \frac{\kappa_0^2}{2\gamma}\right)} \left[sign(\gamma) \left(C\left(\frac{\kappa_0 + \gamma L}{\sqrt{\pi|\gamma|}}\right) \right. \right.
$$
$$
\left. - C\left(\frac{\kappa_0 + \gamma L_1}{\sqrt{\pi|\gamma|}}\right) \right) + i \left(S\left(\frac{\kappa_0 + \gamma L}{\sqrt{\pi|\gamma|}}\right) \right.
$$
$$
\left. \left. - S\left(\frac{\kappa_0 + \gamma L_1}{\sqrt{\pi|\gamma|}}\right) \right) \right]
$$
$$
= \mathcal{C}_0 + \sqrt{\frac{\pi}{|\gamma|}} e^{i\left(\theta_0 - \frac{\kappa_0^2}{2\gamma}\right)} \left[sign(\gamma) \left(C\left(\frac{\kappa_0 + \gamma L}{\sqrt{\pi|\gamma|}}\right) \right. \right.
$$
$$
\left. - C\left(\frac{\kappa_0}{\sqrt{\pi|\gamma|}}\right) \right) + i \left(S\left(\frac{\kappa_0 + \gamma L}{\sqrt{\pi|\gamma|}}\right) \right.
$$
$$
\left. \left. - S\left(\frac{\kappa_0}{\sqrt{\pi|\gamma|}}\right) \right) \right]
$$
$$
= \mathcal{C}_2 = \text{LHS}. \tag{20}
$$

This implies that the Euler spiral interpolation between $\mathcal{C}_1$ and $\mathcal{C}_2$ coincides with that between $\mathcal{C}_0$ and $\mathcal{C}_2$. A similar result holds for the interpolation between $\mathcal{C}_0$ and $\mathcal{C}_1$. □

Consider now Euler Spirals $\mathcal{C}^n(s)$, where n is the iteration number and where each spiral is described by its initial point-tangent pair (x_0, y_0, θ_0) and, its two free parameters (κ_0^n, κ_2^n) as described in Proposition 2. Note that $\mathcal{C}^n(L)$ does not necessarily meet $\mathcal{C}_2$, but its end tangent $\theta^n(L) = \theta_2$ is correct by construction. Now, we seek a sequence $\{(\kappa_0^0, \kappa_2^0), (\kappa_0^1, \kappa_2^1), \ldots, (\kappa_0^n, \kappa_2^n), \ldots\}$ where the distance between the second point $\mathcal{C}_2$ and the end point of the spiral $\mathcal{C}^n(L)$ is decreasing, i.e., where the sequence $\|\mathcal{C}_2 - \mathcal{C}^n(L)\|_2$ converges to zero. Note that $E = 0$ if and only if the interpolating Euler Spiral is obtained. In Section 4, we analytically obtain a biarc interpolant which gives the initial conditions (κ_0^0, κ_2^0). Since the biarc is a close approximation of the Euler Spiral, in practice only a few iterations are necessary for convergence.

4. Biarc Construction and Interpolation

We now examine a solution of the geometric interpolation between two point-tangent pairs in terms of *biarcs*. The curvature of a biarc is piecewise constant and as such it is an approximation to the linear curvature variations of the Euler Spiral. In fact we shall see that the biarc which minimizes curvature variation, i.e., curvature difference between its arcs while satisfying the boundary conditions is a rather close approximation of the Euler Spiral. The analytic formulas we derive here enable it to be used as an initial condition for the derivation of the Euler Spiral in a numerical scheme.

Specifically, consider that the construction of a biarc requires seven parameters: an initial point-tangent pair as well as the curvature and lengths of each arc constrains the parameters of the biarc so that it passes through two points with prescribed tangents, consumes six degrees of freedom, giving rise to a one parameter family of biarcs which interpolate two point-tangent pairs. We will then analytically derive the biarc with
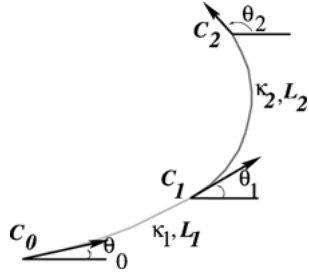
Figure 9. This figure illustrates the biarc interpolation between the point-tangent pair $(C_0(x_0, y_0), \theta_0)$ and $(C_2(x_2, y_2), \theta_2)$. The point where the two arcs come together is not specified appriori.

minimum total curvature variation and use it as the initial estimate for the Euler spiral.

4.1. Biarc Construction

Consider the construction of a biarc given an initial point and orientation (x_0, y_0, θ_0) and the curvatures and lengths corresponding to the two circular arcs from which a biarc is composed $(\kappa_1, L_1, \kappa_2, L_2)$, Fig. 9. Let s denote arclength. Assuming $\kappa_1 \neq 0$, the first arc is constructed by means of:

$$\begin{cases} x(s) = x_0 + \dfrac{1}{\kappa_1}\left(\sin(\kappa_1 s + \theta_0) - \sin\theta_0\right) \\ y(s) = y_0 - \dfrac{1}{\kappa_1}\left(\cos(\kappa_1 s + \theta_0) - \cos\theta_0\right) \\ \text{for } 0 \leq s \leq L_1, \end{cases} \quad (21)$$

and similarly assuming that $\kappa_2 \neq 0$, the second arc using the end point of the first arc,

$$\begin{cases} x(s) = \left(x_0 + \dfrac{1}{\kappa_1}(\sin(\kappa_1 L_1 + \theta_0) - \sin\theta_0)\right) \\ \qquad + \dfrac{1}{\kappa_2}(\sin(\kappa_2(s - L_1) + \theta_1) - \sin\theta_1) \\ \qquad\qquad\qquad \text{for } L_1 \leq s \leq L_1 + L_2, \\ y(s) = \left(y_0 - \dfrac{1}{\kappa_1}(\cos(\kappa_1 L_1 + \theta_0) - \cos\theta_0)\right) \\ \qquad - \dfrac{1}{\kappa_2}(\cos(\kappa_2(s - L_1) + \theta_1) - \cos\theta_1) \end{cases}$$
$$(22)$$

where θ_1 is the tangent angle at the join between the biarc's constituent circular arcs. This angle can be de-

rived using the formula for the tangent angle at an arbitrary point on the biarc:

$$\begin{cases} \theta(s) = \kappa_1 s + \theta_0, & \text{for } 0 \leq s \leq L_1, \\ \theta(s) = \kappa_2(s - L_1) + \theta_1, & \text{for } L_1 \leq s \leq L_1 + L_2. \end{cases}$$
$$(23)$$

Thus, $\theta_1 =_{2\pi} \kappa_1 L_1 + \theta_0$, where $=_{2\pi}$ denotes equality modulo 2π. Note that as κ_1 approaches 0, Eq. (21) in the limit is simplified as

$$\begin{cases} x(s) = x_0 + s\cos\theta_0 \\ y(s) = y_0 + s\sin\theta_0, \end{cases}$$

i.e., the equation for a line. Similarly, as κ_2 approaches 0, Eq. (22) is rewritten as

$$\begin{cases} x(s) = \left(x_0 + \dfrac{1}{\kappa_1}(\sin(\kappa_1 L_1 + \theta_0) - \sin\theta_0)\right) \\ \qquad + (s - L_1)\cos\theta_1 \\ \qquad\qquad\qquad\quad \text{for } L_1 \leq s \leq L_1 + L_2. \\ y(s) = \left(y_0 - \dfrac{1}{\kappa_1}(\cos(\kappa_1 L_1 + \theta_0) - \cos\theta_0)\right) \\ \qquad + (s - L_1)\sin\theta_1 \end{cases}$$

This is the complete specification of a biarc using *seven* parameters $(x_0, y_0, \theta_0, \kappa_1, L_1, \kappa_2, L_2)$. Note that $L_1 > 0$ and $L_2 > 0$ while curvatures κ_1 and κ_2 can take any finite value.

4.2. A Family of Biarc Interpolants

We now identify the biarcs which satisfy the boundary conditions, i.e., pass through a pair of points with specified tangents. Since there are six constraints and seven variables, multiple biarcs can possibly satisfy these conditions. Thus, we characterize the set of solutions as a (one-parameter) family and then use the minimum curvature variation criterion to find the optimal biarc interpolation.

Problem Statement: Given two point-tangent pairs, $C_0(x_0, y_0, \theta_0)$ and $C_2(x_2, y_2, \theta_2)$,[8] find the *smoothest* biarc $(x_0, y_0, \theta_0, \kappa_1, L_1, \kappa_2, L_2)$ which passes through said points at their respective tangents.

Proposition 5. *Consider two endpoints with associated tangents $C_0(x_0, y_0, \theta_0)$ and $C_2(x_2, y_2, \theta_2)$, and denote $C_2 - C_0 = L_0 e^{i\psi}$ as before. Then, the set of biarcs*

which satisfy these boundary conditions can be parameterized by the curvature of the first arc, κ_1, where the remaining parameters (κ_2, L_1, L_2) are analytically derived separately for four conditions:

(i) $\kappa_1 = \kappa_2 = 0$; this happens only if $\theta_0 = \theta_2 = \psi$ and $L = L_1 + L_2 = L_0$;

(ii) $\kappa_1 = 0, \kappa_2 \neq 0$. In this case, $\theta_0 \neq \theta_2$, $\theta_0 \neq \psi$, and

$$\kappa_2 = \frac{-2}{L_0} \frac{\sin^2\left(\frac{\theta_2 - \theta_0}{2}\right)}{\sin(\theta_0 - \psi)},$$
$$L_1 = L_0 \frac{\sin\left(\frac{\theta_2 + \theta_0}{2} - \psi\right)}{\sin\left(\frac{\theta_0 - \theta_2}{2}\right)} \qquad (24)$$
$$L_2 = \frac{\theta_2 - \theta_0}{\kappa_2} + 2n\pi,$$

where n is chosen to give the smallest positive L_2;

(iii) $\kappa_1 \neq 0, \kappa_2 = 0$; we have $\theta_0 \neq \theta_2$, $\theta_2 \neq \psi$ and

$$\kappa_1 = \frac{2 \sin^2\left(\frac{\theta_2 - \theta_0}{2}\right)}{\sin(\theta_2 - \psi)}$$
$$L_1 = \frac{\theta_2 - \theta_0}{\kappa_1} + 2n\pi, \qquad (25)$$
$$L_2 = L_0 \frac{\sin\left(\frac{\theta_2 + \theta_0}{2} - \psi\right)}{\sin\left(\frac{\theta_0 - \theta_2}{2}\right)},$$

where n is chosen to give the smallest positive L_1.

(iv) $\kappa_1 \neq 0$ and $\kappa_2 \neq 0$; In this case, if $\kappa_1 \neq \kappa_2$, then not all θ_0, θ_2, ψ are equal and

$$\kappa_2 = \frac{2}{L_0} \frac{-2 \sin^2\left(\frac{\theta_2 - \theta_0}{2}\right) + \kappa_1 L_0 \sin(\theta_2 - \psi)}{2 \sin(\theta_0 - \psi) + \kappa_1 L_0},$$
$$L_1 = \frac{\theta_1 - \theta_0 + 2n_1 \pi}{\kappa_1}, \qquad (26)$$
$$L_2 = \frac{\theta_2 - \theta_1 + 2n_2 \pi}{\kappa_2},$$

where n_1 and n_2 are chosen to give the smallest positive L_1 and L_2, respectively, and where θ_1 is defined as:

$$\begin{cases} \sin\theta_1 = \dfrac{\kappa_1 \kappa_2 (x_2 - x_0) + \kappa_2 \sin\theta_0 - \kappa_1 \sin\theta_2}{\kappa_2 - \kappa_1} \\[2mm] \cos\theta_1 = \dfrac{-\kappa_1 \kappa_2 (y_2 - y_0) + \kappa_2 \cos\theta_0 - \kappa_1 \cos\theta_2}{\kappa_2 - \kappa_1}. \end{cases}$$
$$(27)$$

On the other hand, if $\kappa_1 = \kappa_2$, then $\theta_0 \neq \theta_2$, $\psi = \frac{\theta_0 + \theta_2}{2}$ and the biarc degenerates to a single arc with curvature and length

$$\kappa_1 = \kappa_2 = \frac{2}{L_0} \sin\left(\frac{\theta_2 - \theta_0}{2}\right),$$
$$L = L_1 + L_2 = L_0 \frac{\left(\frac{\theta_2 - \theta_0}{2}\right)}{\sin\left(\frac{\theta_2 - \theta_0}{2}\right)}. \qquad (28)$$

Proof: Since the constraints pertaining to the initial oriented point $\mathcal{C}_0$ are implicitly satisfied by the forward construction of the biarc, those pertaining to $\mathcal{C}_2$ are satisfied when the coordinates defined by Eq. (22) at L are (x_2, y_2) and the tangent angle defined by Eq. (23) at $L = L_1 + L_2$ is θ_2. First, when $\kappa_1 \neq 0$ and $\kappa_2 \neq 0$

$$\begin{cases} x_2 = x_0 + \dfrac{1}{\kappa_1}(\sin(\kappa_1 L_1 + \theta_0) - \sin\theta_0) \\ \qquad + \dfrac{1}{\kappa_2}(\sin\theta_2 - \sin(\kappa_1 L_1 + \theta_0)) \\ y_2 = y_0 - \dfrac{1}{\kappa_1}(\cos(\kappa_1 L_1 + \theta_0) - \cos\theta_0) \\ \qquad - \dfrac{1}{\kappa_2}(\cos\theta_2 - \cos(\kappa_1 L_1 + \theta_0)) \\ \theta_2 =_{2\pi} \kappa_2 L_2 + \kappa_1 L_1 + \theta_0. \end{cases} \qquad (29)$$

The set of three equations in Eq. (29) constrains the four unknowns $(\kappa_1, L_1, \kappa_2, L_2)$ but lacks one equation to solve for them. However, the set of solutions can be characterized by parameterizing them in terms of some variable. Observe an interesting asymmetry in the relationships among $\kappa_1, L_1, \kappa_2, L_2$, namely, that κ_1 and κ_2 correlate independently of L_1 and L_2. Assuming $\kappa_1 \neq \kappa_2$,

$$\begin{cases} (x_2 - x_0) + \left(\dfrac{1}{\kappa_1}\sin\theta_0 - \dfrac{1}{\kappa_2}\sin\theta_2\right) \\ \quad = \left(\dfrac{1}{\kappa_1} - \dfrac{1}{\kappa_2}\right)\sin\theta_1 \\ (y_2 - y_0) - \left(\dfrac{1}{\kappa_1}\cos\theta_0 - \dfrac{1}{\kappa_2}\cos\theta_2\right) \\ \quad = -\left(\dfrac{1}{\kappa_1} - \dfrac{1}{\kappa_2}\right)\cos\theta_1. \end{cases} \qquad (30)$$

In the general case when $\kappa_1 \neq 0$, $\kappa_2 \neq 0$, and $\kappa_1 \neq \kappa_2$, κ_1 can be chosen as the independent parameter, and κ_2, L_1, L_2 can be found as functions of κ_1. Special cases which violate one or more of these conditions are also handled after considering the general case.

First, in the general case θ_1 can be eliminated from Eq. (30)

$$\left((x_2 - x_0) + \left(\frac{1}{\kappa_1} \sin\theta_0 - \frac{1}{\kappa_2} \sin\theta_2\right)\right)^2$$
$$+ \left((y_2 - y_0) - \left(\frac{1}{\kappa_1} \cos\theta_0 - \frac{1}{\kappa_2} \cos\theta_2\right)\right)^2$$
$$= \left(\frac{1}{\kappa_1} - \frac{1}{\kappa_2}\right)^2.$$

Expanding, and using $x_2 - x_0 = L_0 \cos\psi$ and $y_2 - y_0 = L_0 \sin\psi$, we solve for κ_2 in terms of κ_0,

$$\kappa_2 = \frac{2}{L_0} \frac{-2\sin^2\left(\frac{\theta_2 - \theta_0}{2}\right) + \kappa_1 L_0 \sin(\theta_2 - \psi)}{2\sin(\theta_0 - \psi) + \kappa_1 L_0} \quad (31)$$

Thus, κ_2 is computable in terms of κ_1 independent of L_1 or L_2. Note that when $\kappa_1 = \frac{-2}{L_0} \sin(\theta_0 - \psi)$, $|\kappa_2| = \infty$. Equation (30) also solves for θ_1, in terms of κ_1

$$\begin{cases} \sin\theta_1 = \dfrac{\kappa_1 \kappa_2 (x_2 - x_0) + \kappa_2 \sin\theta_0 - \kappa_1 \sin\theta_2}{\kappa_2 - \kappa_1} \\ \cos\theta_1 = \dfrac{-\kappa_1 \kappa_2 (y_2 - y_0) + \kappa_2 \cos\theta_0 - \kappa_1 \cos\theta_2}{\kappa_2 - \kappa_1}, \end{cases}$$
$$(32)$$

Since $\theta_1 = \kappa_1 L_1 + \theta_0 + 2n_1\pi$, multiple solutions are possible corresponding to arcs which wind more than 2π. We seek the smallest positive L_1 by selecting n_1 as follows,

$$\begin{cases} n_1 = 0 & \theta_1 - \theta_0 > 0 \quad \text{and} \quad \kappa_1 > 0 \\ n_1 = +1 & \theta_1 - \theta_0 > 0 \quad \text{and} \quad \kappa_1 < 0 \\ n_1 = -1 & \theta_1 - \theta_0 < 0 \quad \text{and} \quad \kappa_1 > 0 \\ n_1 = 0 & \theta_1 - \theta_0 < 0 \quad \text{and} \quad \kappa_1 < 0. \end{cases} \quad (33)$$

Similarly,

$$L_2 = \frac{\theta_2 - \theta_1 + 2n_2\pi}{\kappa_2}, \quad (34)$$

which solves for L_2 in the manner described above. In summary, Eqs. (31) through 34 solve for κ_2, L_1, L_2 in terms of κ_1, when $\kappa_1 \neq 0, \kappa_2 \neq 0$ and $\kappa_1 \neq \kappa_2$, and ensure that all the constraints in Eq. (29) are met.

We now consider a special case where $\kappa_1 = \kappa_2 \neq 0$. From Eq. (29) we have

$$\begin{cases} x_2 - x_0 = (-\sin\theta_0 + \sin\theta_2)\dfrac{1}{\kappa_2} \\ y_2 - y_0 = (\cos\theta_0 - \cos\theta_2)\dfrac{1}{\kappa_2} \end{cases} \quad (35)$$

Note that this implies $\theta_0 \neq \theta_2$, since the points $\mathcal{C}_0$ and $\mathcal{C}_2$ are distinct. Recall that $(x_2 - x_0, y_2 - y_0) = L_0(\cos\psi, \sin\psi)$, so that Eq. (35) can be rewritten as

$$\begin{cases} L_0 \cos\psi = \dfrac{2}{\kappa_2} \sin\left(\dfrac{\theta_2 - \theta_0}{2}\right) \cos\left(\dfrac{\theta_2 + \theta_0}{2}\right) \\ L_0 \sin\psi = \dfrac{2}{\kappa_2} \sin\left(\dfrac{\theta_2 - \theta_0}{2}\right) \sin\left(\dfrac{\theta_2 + \theta_0}{2}\right) \end{cases} \quad (36)$$

or, equivalently, $\tan\psi = \tan\frac{\theta_2 + \theta_0}{2}$. It follows that to have equal curvatures κ_1 and κ_2, i.e, when the biarc degenerates to a circular arc, we must have $\psi = \frac{\theta_0 + \theta_2}{2} + n\pi$. Note that when $\theta_0 + \theta_2 = \pi$, the same relationship holds. Substituting back into Eq. (36) gives:

$$\begin{cases} (-1)^n L_0 \cos\left(\dfrac{\theta_0 + \theta_2}{2}\right) \\ \quad = \dfrac{2}{\kappa_2} \sin\left(\dfrac{\theta_2 - \theta_0}{2}\right) \cos\left(\dfrac{\theta_0 + \theta_2}{2}\right) \\ (-1)^n L_0 \sin\left(\dfrac{\theta_0 + \theta_2}{2}\right) \\ \quad = \dfrac{2}{\kappa_2} \sin\left(\dfrac{\theta_2 - \theta_0}{2}\right) \sin\left(\dfrac{\theta_0 + \theta_2}{2}\right) \end{cases} \quad (37)$$

Thus,

$$\kappa_1 = \kappa_2 = (-1)^n \frac{2}{L_0} \sin\left(\frac{\theta_2 - \theta_0}{2}\right), \quad (38)$$

where n is decided from the relationship between ψ and $\frac{\theta_0 + \theta_2}{2}$. The lengths are obtained from Eq. (29),

$$\theta_2 = \kappa_1(L_1 + L_2) + \theta_0$$
$$= (-1)^n \frac{2}{L_0} \sin\left(\frac{\theta_2 - \theta_0}{2}\right)(L_1 + L_2) + \theta_0.$$

Thus, the total length is

$$L = L_1 + L_2 = \frac{L_0}{2} \frac{(-1)^n \left(\frac{\theta_2 - \theta_0}{2}\right)}{\sin\left(\frac{\theta_2 - \theta_0}{2}\right)}. \quad (39)$$

Since L must be positive, this further constrains the required relationship among ψ, θ_0 and θ_2 when curvatures are equal, namely $n = 0$:

(i) if $\theta_2 - \theta_0 > 0$ then $0 < \frac{\theta_2 - \theta_0}{2} < \pi$ and $\frac{\frac{\theta_2 - \theta_0}{2}}{\sin \frac{\theta_2 - \theta_0}{2}} > 0$ requiring $n = 0$;

(ii) if $\theta_2 - \theta_0 < 0$ then $-\pi < \frac{\theta_2 - \theta_0}{2} < 0$ and $\frac{\frac{\theta_2 - \theta_0}{2}}{\sin \frac{\theta_2 - \theta_0}{2}} > 0$ requiring $n = 0$.

Hence, $\psi = \frac{\theta_0 + \theta_2}{2}$, and $\kappa_1 = \kappa_2 = \frac{2}{L_0} \sin \frac{\theta_2 - \theta_0}{2}$, $L = \frac{L_0}{2} \frac{\frac{\theta_2 - \theta_0}{2}}{\sin \frac{\theta_2 - \theta_0}{2}}$.

Note, further, that in the limit as $\theta_2 = \theta_0$, then $\kappa_2 = \kappa_1 = 0$ (straight line) and $L_1 + L_2 = L_0$, as expected. This completes the proof of case (iv).

Let's now consider the special case (ii) when $\kappa_1 = 0$, $\kappa_2 \neq 0$. Equation (29) gives

$$\begin{cases} x_2 = x_0 + L_1 \cos \theta_0 + \dfrac{\sin \theta_2 - \sin \theta_0}{\kappa_2} \\ y_2 = y_0 + L_1 \sin \theta_0 - \dfrac{\cos \theta_2 - \cos \theta_0}{\kappa_2}, \end{cases} \quad (40)$$

which gives two equations in two unknowns L_1 and κ_2. If $\theta_2 = \theta_0$, this equation requires $\psi = \theta_0$, which forces $\kappa_1 = \kappa_2 = 0$, thus violating this case's assumption. Thus, $\theta_2 \neq \theta_0$. Similarly, $\psi = \theta_0$ leads to $\theta_2 = \theta_0$, so this is also not possible. Eliminating κ_2 from Eq. (40) and solving for L leads to

$$L_1 = L_0 \frac{\sin\left(\frac{\theta_0 + \theta_2}{2} - \psi\right)}{\sin\left(\frac{\theta_2 - \theta_0}{2}\right)}. \quad (41)$$

The expression for κ_2 is then either derived from the limiting case of Eq. (31) or directly by eliminating L_1 in Eq. (40) as:

$$\kappa_2 = \frac{-2}{L_0} \frac{\sin^2\left(\frac{\theta_2 - \theta_0}{2}\right)}{\sin(\theta_0 - \psi)}. \quad (42)$$

The third case (iii) is handled similarly. Finally, in case (i), when $\kappa_1 = \kappa_2 = 0$, the biarc degenerates to a single line requiring $\theta_0 = \theta_2 = \psi$. In this case, $L = L_1 + L_2 = L_0$. This completes the proof in all cases.

Corollary 1.   *Given the conditions of Proposition 4, we have the following cases*:
(a) *if $\theta_0 = \theta_2 = \psi$ then $\kappa_0 = \kappa_2 = 0$ and $L = L_0$;*
(b) *if $\theta_0 = \theta_2 \neq \psi$ then only case* (iv) *applies with $\theta_0 = \theta_2$.*

(c) *if $\theta_0 \neq \theta_2$ and $\psi = \frac{\theta_0 + \theta_2}{2}$, then the biarc degenerates to an arc, $\kappa_1 = \kappa_2$ and Eq. (28) of case* (iv) *applies;*
(d) *if $\theta_0 \neq \theta_2$ and $\psi \neq \frac{\theta_0 + \theta_2}{2} + n\pi$, then*

(d.1) *if $\psi = \theta_0$, cases* (iii) *and* (iv) *are possible,*
(d.2) *if $\psi = \theta_2$, cases* (ii) *and* (iv) *are both possible, and*
(d.3) *if $\psi = \theta_0$ and $\psi = \theta_2$, then cases* (ii), (iii) *and* (iv) *are all possible.*

4.3.   Optimal Biarc Interpolation

Proposition 4 characterizes the set of biarcs satisfying the point-tangent boundary conditions. The selection of the optimal biarc requires an additional constraint. In contrast to Ullman's constraint of minimizing total squared curvature, we will use the constraint of minimizing the total curvature variation, Eq. (3). Since the circular arcs themselves have no curvature variation, minimizing the integral in Eq. (3) is tantamount to minimizing the difference in arc curvatures $(\kappa_2 - \kappa_1)^2$ at the point joining them.

Proposition 6.   *The optimal biarc, i.e., the biarc minimizing total curvature variation $E = (\kappa_2 - \kappa_1)^2$, and satisfying endpoint tangent conditions $\mathcal{C}_0(x_0, y_0, \theta_0)$ and $\mathcal{C}_2(x_2, y_2, \theta_2)$ is specified as follows*:

(a) *if $\psi = \frac{\theta_0 + \theta_2}{2}$ then the optimal biarc degenerates to a circular arc*

$$\kappa_1 = \kappa_2 = \frac{2}{L_0} \sin \frac{\theta_2 - \theta_0}{2}, \quad (43)$$

with $E = 0$. The approximation for L when $\theta_0 \neq \theta_2$, is

$$L = L_1 + L_2 = L_0 \frac{\frac{\theta_2 - \theta_0}{2}}{\sin\left(\frac{\theta_2 - \theta_0}{2}\right)}, \quad (44)$$

while, if $\theta_0 = \theta_2$, then $L = L_0$.
(b) *if $\psi \neq \frac{\theta_0 + \theta_2}{2}$ and $\theta_0 \neq \theta_2$, then two extremal solutions exist. When $|\theta_2 - \theta_0| > \pi$ the solution is*

$$\begin{cases} \kappa_1 = \dfrac{-4}{L_0} \sin\left(\dfrac{3\theta_0 + \theta_2}{4} - \psi\right) \cos\left(\dfrac{\theta_2 - \theta_0}{4}\right) \\ \kappa_2 = \dfrac{4}{L_0} \sin\left(\dfrac{\theta_0 + 3\theta_2}{4} - \psi\right) \cos\left(\dfrac{\theta_2 - \theta_0}{4}\right), \end{cases}$$
$$(45)$$

with $E_1 = \frac{64}{L_0^2} \cos^4(\frac{\theta_2 - \theta_0}{4}) \sin^2(\frac{\theta_0 + \theta_2}{2} - \psi)$, and with L_1 and L_2 specified by Eq. (26). When $0 < |\theta_2 - \theta_0| < \pi$

$$\begin{cases} \kappa_1 = \frac{4}{L_0} \cos\left(\frac{3\theta_0 + \theta_2}{4} - \psi\right) \sin\left(\frac{\theta_2 - \theta_0}{4}\right) \\ \kappa_2 = \frac{4}{L_0} \cos\left(\frac{\theta_0 + 3\theta_2}{4} - \psi\right) \sin\left(\frac{\theta_2 - \theta_0}{4}\right), \end{cases}$$
(46)

with $E_2 = \frac{64}{L_0^2} \sin^4(\frac{\theta_2 - \theta_0}{4}) \sin^2(\frac{(\theta_0 + \theta_2)}{2} - \psi)$, and with L_1 and L_2 obtained from Eq. (26).

(c) if $\psi \neq \frac{\theta_0 + \theta_2}{2}$ and $\theta_0 = \theta_2$, then the solution is an "S-curve",

$$\begin{cases} \kappa_1 = \frac{-4}{L_0} \sin(\theta_0 - \psi) \\ \kappa_2 = \frac{4}{L_0} \sin(\theta_0 - \psi), \end{cases}$$
(47)

with $E = \frac{64}{L_0^2} \sin^2(\theta_0 - \psi)$.

Proof: First, in case(a) where $\psi = \frac{\theta_0 + \theta_2}{2}$, from Proposition 3 cases (i) and the second part of (iv) are valid, and the family of biarcs degenerates to a single arc solution: if $\theta_0 = \theta_2$ this is a straight line $\kappa_1 = \kappa_2 = 0$; otherwise, if $\theta_0 \neq \theta_2$, curvatures of the arc are obtained from Eq. (28). Thus the optimal biarc is the only biarc.

Second, consider the case where $\psi \neq \frac{\theta_0 + \theta_2}{2}$. Then, curvature κ_2 can be written as in Eq. (26) covering not only the first part of case (iv) but also cases (ii) and (iii) as special cases. Note that in all cases $\kappa_1 \neq \kappa_2$. Analytically, optimizing $E = (\kappa_2 - \kappa_1)^2$ requires that $\frac{dE}{d\kappa_1} = 0$, or $2(\kappa_2 - \kappa_1)\frac{d}{d\kappa_1}(\kappa_2 - \kappa_1) = 0$ which can happen only if $\frac{d\kappa_2}{d\kappa_1} = 1$,

$$\begin{aligned} \frac{d\kappa_2}{d\kappa_1} &= \frac{2}{L_0} \frac{1}{(2\sin(\theta_0 - \psi) + \kappa_1 L_0)^2} L_0 \sin(\theta_2 - \psi) \\ &\quad \times (2\sin(\theta_0 - \psi) + \kappa_1 L_0) \\ &\quad - L_0(-1 + \cos(\theta_2 - \theta_0) + \kappa_1 L_0 \sin(\theta_2 - \psi)) \\ &= \frac{2}{(2\sin(\theta_0 - \psi) + \kappa_1 L_0)^2} \\ &\quad \times (2\sin(\theta_2 - \psi)\sin(\theta_0 - \psi) \\ &\quad + 1 - \cos(\theta_2 - \theta_0)) \\ &= \left(\frac{2\sin(\frac{\theta_0 + \theta_2}{2} - \psi)}{2\sin(\theta_0 - \psi) + \kappa_1 L_0}\right)^2, \end{aligned}$$
(48)

leading to two solutions

$$\frac{2\sin(\frac{\theta_0 + \theta_2}{2} - \psi)}{2\sin(\theta_0 - \psi) + \kappa_1 L_0} = \pm 1.$$
(49)

The first solution corresponding to the negative sign is

$$\kappa_1 = -\frac{2}{L_0}\left(\sin\left(\frac{\theta_0 + \theta_2}{2} - \psi\right) + \sin(\theta_0 - \psi)\right)$$

$$= -\frac{4}{L_0} \sin\left(\frac{3\theta_0 + \theta_2}{4} - \psi\right) \cos\left(\frac{\theta_2 - \theta_0}{4}\right) \quad (50)$$

From this value for κ_1 and from Eq. (31), and some more manipulation,

$$\kappa_2 = \frac{4}{L_0} \sin\left(\frac{\theta_0 + 3\theta_2}{4} - \psi\right) \cos\left(\frac{\theta_2 - \theta_0}{4}\right). \quad (51)$$

Note that in this case

$$\kappa_2 - \kappa_1 = \frac{8}{L_0} \cos^2\left(\frac{\theta_2 - \theta_0}{4}\right) \sin\left(\frac{\theta_0 + \theta_2}{2} - \psi\right).$$
(52)

Similarly, the second solution corresponding to the positive sign in Eq. (49) gives

$$\begin{cases} \kappa_1 = \frac{4}{L_0} \cos\left(\frac{3\theta_0 + \theta_2}{4} - \psi\right) \sin\left(\frac{\theta_2 - \theta_0}{4}\right), \\ \kappa_2 = \frac{4}{L_0} \cos\left(\frac{\theta_0 + 3\theta_2}{4} - \psi\right) \sin\left(\frac{\theta_2 - \theta_0}{4}\right). \end{cases}$$
(53)

For this second solution,

$$\kappa_2 - \kappa_1 = -\frac{8}{L_0} \sin^2\left(\frac{\theta_2 - \theta_0}{4}\right) \sin\left(\frac{\theta_0 + \theta_2}{2} - \psi\right).$$
(54)

Having characterized the only two solutions at which the derivative of E is zero, we now examine whether these extrema are minima, by verifying that $\frac{dE^2}{d\kappa_1^2} > 0$. Since

$$\frac{d^2 E}{d\kappa_1^2} = 2\left(\frac{d\kappa_2}{d\kappa_1} - 1\right)^2 + 2(\kappa_2 - \kappa_1)\frac{d^2\kappa_2}{d^2\kappa_1}, \quad (55)$$

$$= 2(\kappa_2 - \kappa_1)\frac{d^2\kappa_2}{d^2\kappa_1}. \quad (56)$$

Taking second derivatives using Eq. (48) and then using Eq. (49),

$$\frac{d^2\kappa_2}{d^2\kappa_1} = -2L_0 \frac{4\sin^2\left(\frac{\theta_0+\theta_2}{2} - \psi\right)}{(2\sin(\theta_0 - \psi) + \kappa_1 L_0)^3}$$

$$= \pm \frac{-L_0}{\sin\left(\frac{\theta_0+\theta_2}{2} - \psi\right)}. \tag{57}$$

Now for the first solution, we obtain $\frac{d^2E}{d^2\kappa_1} = 16\cos^2(\frac{\theta_2-\theta_0}{4})$ while for the second solution $\frac{d^2E}{d^2\kappa_1} = 16\sin^2(\frac{\theta_2-\theta_0}{4})$.

We conclude that the solutions are local minima, except possibly for the second solution when $\theta_0 = \theta_2$. This special case is considered below. The global minimum is the choice between the two with a lower $E = (\kappa_2-\kappa_1)^2$. Thus, when $|\theta_2-\theta_0| < \pi$, $\sin^2(\frac{\theta_2-\theta_0}{4}) < \cos^2(\frac{\theta_2-\theta_0}{4})$ and the second solution is the lower minimum, while when $|\theta_2 - \theta_0| > \pi$, the first solution is the better one.

Finally, consider the special case when $\theta_0 = \theta_2$. The first solution corresponding to the negative sign is

$$\kappa_1 = \frac{-4}{L_0}\sin(\theta_0 - \psi),$$
$$\kappa_2 = \frac{4}{L_0}\sin(\theta_0 - \psi), \tag{58}$$

which corresponds to an "S-shaped curve" biarc consisting of two identical arcs of equal curvature but opposite sign. In this case

$$\kappa_2 - \kappa_1 = \frac{8}{L_0}\sin(\theta_0 - \psi). \tag{59}$$

The second solution gives $\kappa_1 = 0$ and $\kappa_2 = 0$, but the latter violates the assumption that $\kappa_1 \neq \kappa_2$.[9]   □

Corollary 2. *The optimal biarc interpolating between $\mathcal{C}_0(x_0, y_0, \theta_0)$ and $\mathcal{C}_2(x_2, y_2, \theta_2)$ degenerates to a circular arc if and only if the point-tangent pairs are co-circular.*

Proof: When two tangents lie on a circle, $\psi = \theta_0 + \frac{\theta_2-\theta_0}{2} = \frac{\theta_2+\theta_0}{2}$, and we have a single arc. We can also check the limiting case of the solution as $\psi \to \frac{\theta_0+\theta_2}{2}$

$$\kappa_1 = \frac{-4}{L_0}\sin\left(\frac{3\theta_0+\theta_2}{4} - \frac{\theta_2+\theta_0}{2}\right)\cos\left(\frac{\theta_2-\theta_0}{4}\right)$$

$$= \pm\frac{2}{L_0}\sin\frac{(\theta_2-\theta_0)}{2}.$$

A similar argument for κ_2 shows that the limit of κ_2 is the limit of κ_1. On the other hand, if $\kappa_1 = \kappa_2$, suppose $\psi \neq \frac{\theta_0+\theta_2}{2}$. Then, for the first solution $2\sin(\frac{\theta_0+\theta_2}{2} - \psi)\cos(\frac{\theta_2-\theta_0}{4}) = 0$. Since both θ_0 and θ_2 are in the range $[0, 2\pi)$, the only term which can be zero is $\sin(\frac{\theta_0+\theta_2}{2} - \psi)$, and therefore $\psi = \frac{\theta_2+\theta_0}{2} + n\pi$. In order to have positive length, n must be zero. A similar argument holds for the second solution. Thus, $\psi = \frac{\theta_2+\theta_0}{2}$, a contradiction, and the tangents must be co-circular.   □

The pseudocode for biarc interpolation is described in Appendix A.1.

5.   Examples

In this section we examine the Euler spiral completion curve for a variety of point-tangent configurations, probe the extensibility property of the Euler Spiral, and apply the results to the examples presented in the introduction, Fig. 1. We will then describe how this approach may be used in several computer vision tasks, specifically, disambiguating edge maps in perceptual grouping, partitioning visual form, and the filling-in of occluded areas.

The completion curve is derived by analytically finding the optimal biarc as described in Section 4, and then using gradient descent using the biarc as the initial condition to solve the nonlinear optimization described in Section 2 (see also Appendix A.2), as demonstrated in Fig. 10.

The completion curve is shown for a variety of point-tangent pair configurations in Fig. 11. A subjective examination reveals that the completion curve is intuitive and natural. Figure 12 shows this completion curve when overlayed on synthetic occluders; both the final Euler spiral and the intermediate biarc are shown; observe that the biarc is a good approximation of the Euler spiral. Figure 13 shows the completion curve for the Kanizsa illusory contour, the occluded kangaroo, and for other shapes.

The extensibility property of the completion curve is examined in Fig. 14. Observe that the numerically derived completion curve satisfies the extensibility property as predicted by the theoretical results. Extensibility of the completion contour is critical in the completion of a boundary behind an occluder, i.e., the completion curve remains stable with changes in the extent of the occlusion. Note that elastica are extensible, but
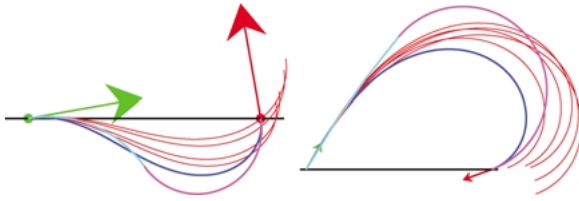
Figure 10. Two examples of how the initial biarc (in cyan and magenta), gives rise to a series of Euler Spirals which converge to the Euler Spiral (in blue) using gradient descent. The intermediate spirals are in red.

are not stable with changes in scale. In contrast, scale-invariant version of elastica are stable with change in scale, but are not extensible. The Euler Spiral solution is stable with changes in the extent of occlusion and extensible with changes in scale.

The question naturally arises that while these completions appear intuitive, what role if any can they can potentially play in actual computations required for various computer vision tasks. We now describe three potential uses of the Euler spiral completion curves in this context. First, consider the task of disambiguating

edge maps in perceptual grouping. Since edge detection algorithms often result in imperfect edge maps containing numerous gaps, spurious edges, etc., perceptual grouping is required to disambiguate the edge map by taking into account structural saliency. There are a large number of approaches for accomplishing this. Williams and Thornber (1999) note that in general these approaches involve two steps of first computing a local *affinity measure* for a pair of edges, and then computing a global *saliency measure* by optimizing support over various curve hypotheses (Guy and Medioni, 1992; Herault and Horaud, 1993; Parent and Zucker, 1989; Sarkar and Boyer, 1992; Sharon et al., to appear; Williams and Jacobs, 1997; Williams and Thornber, 1999). While previous approaches have used cocircularity (Parent and Zucker, 1989), and the total curvature of elastical completion curves, we propose that the local affinity measure can instead be based on the properties of the Euler spiral, as used in Johannes et al. (2001) and depicted in Fig. 15.

While all the information pertaining to these properties is already implicit in the part-tangent pairs, the computation of the completion curve properties e.g.,
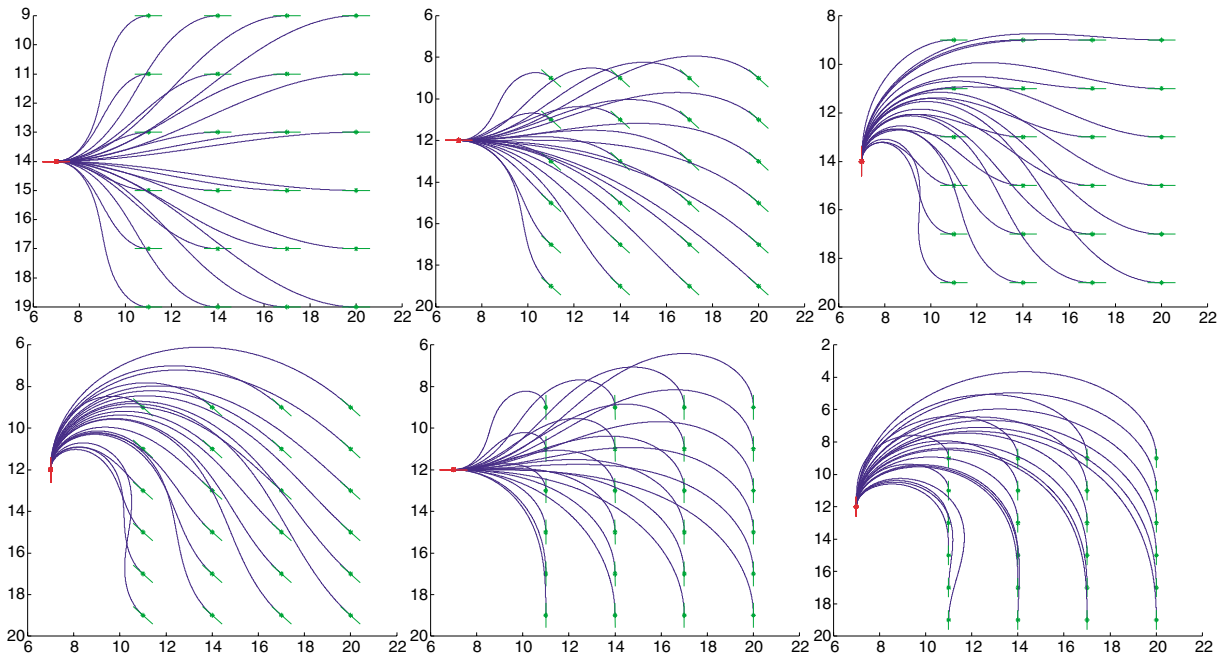

Figure 11. The interpolation of a pair of point-tangent pairs by the Euler Spiral. The first point and its tangent are held constant for each graph while varying the position and tangent at the second point. Note that the entire space of variations can be described by two parameters, i.e., the angle of each tangent with respect to the line connecting them. However, we show examples in this extrinsic setting as the variation at end points is exactly what arises in visual situations. Observe that the completions are visually intuitive.
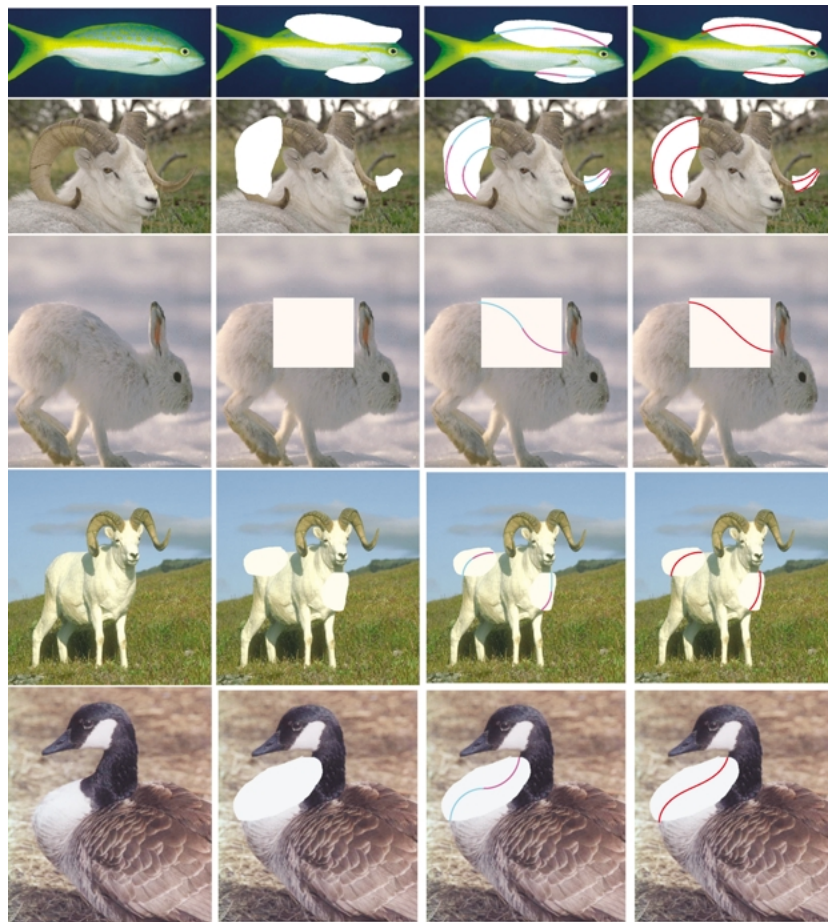
Figure 12.   From left to right, original image, occluded object, biarc completion of the simulated occlusion, Euler spiral refinement of the biarc completion.
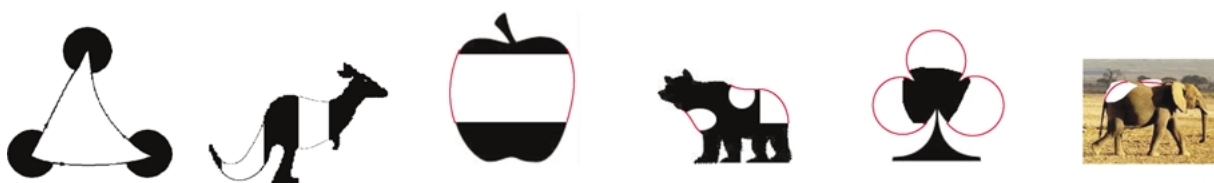

Figure 13.   The completion curve for several examples including two of the examples presented in Fig. 1.

of curvature variation γ, currently requires the explicit reconstruction of the Euler spiral through the biarc as described in Section 4. Furthermore, in connecting two edges, one must verify that the completion curve does not intersect with the existing edges or previously established completion contours, thus arguing for the explicit reconstruction of the Euler spiral, rather than just deriving these properties from the point-tangent pairs.

Second, consider the task of partitioning visual form. While boundary-based approaches partition the silhouettes based on salient features such as negative curvature extrema (Hoffman and Richards, 1985), some region-based schemes look for the suitability of actual "break curves" through the shape which are anchored at these salient features (Siddiqi and Kimia, 1995). Specifically, ambiguous partitioning hypotheses can be disambiguated using a measure of part-curve saliency,
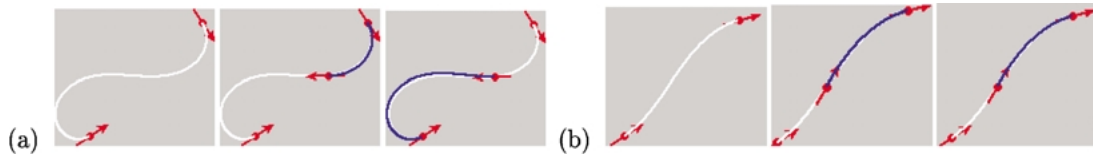
Figure 14. Two examples illustrating that the Euler Spiral is extensible. The blue portion is the interpolation starting with the middle point. Extensibility is critical since the interpolation must be stable with changes in the extent of occlusion.
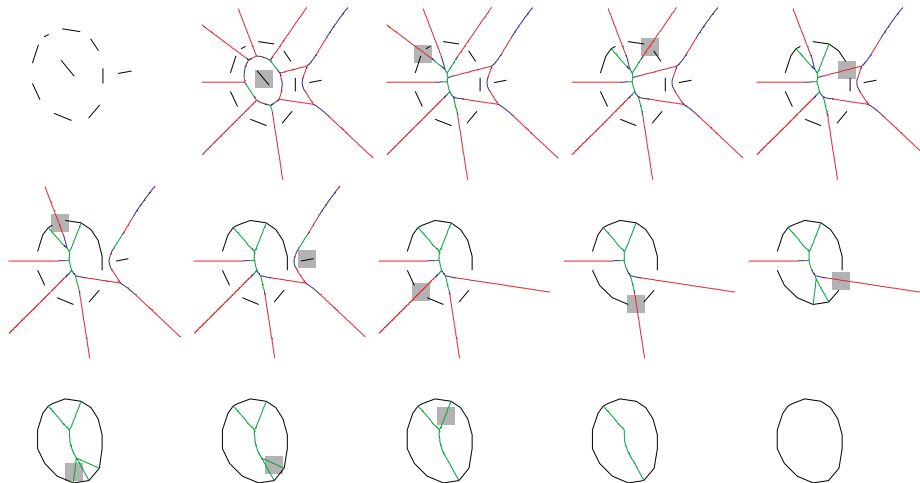

Figure 15. A "circular" shape is embedded among spurious edges. The sequence of operations that either removes an edge or groups it with others is generated by a gradient descent on an energy functional which is based on the energy of the Euler Spiral interpolation between neighboring edge elements (Johannes et al., 2001). The additional curves are the medial axis which indicate which pairs of point-tangent pairs should be considered at each step.

Fig. 16. While the original approach used part-lines to test the inclusion of the break curves inside the shape and splines to measure the total curvature, the Euler spiral completions are more appropriate to use in both tasks (Dhandapani and Kimia, 2002). Again, in analogy to the edge map disambiguation, while this information is implicit in the point-tangent pairs, its computation requires an explicit reconstruction to check that hypothesized break-curves do not intersect the boundary of the shape.

The third example is based on object completion behind an occluder, e.g., as required in in-painting. The current approach to in-painting interpolates intensities in the missing region, thus effectively diffusing boundary intensities within that region. This approach, however, will fail when the missing region contains boundaries, as in Fig. 17, where diffusion-based inpainting smears two different regions together, Fig. 17(c). The explicit reconstruction of the missing boundary prior to the diffusion process, however, prevents this, Fig. 17(d).

6.   Summary and Discussion

The class of curves which interpolate two point-tangent pairs, i.e., by passing through each point with specified tangents, is rather large. Thus, some criterion is required to pick the most suitable curve to interpolate between them. Previously, several measures of optimality have been proposed that attempt to capture our sense of aesthetics and how pleasing the interpolation curve appears. In addition, in previous approaches restricted classes of curves such as biarcs or cubic splines have been identified that render the optimization practical.

Despite such ambiguity and the apparent lack of guidelines in the selection of an optimality measure and an appropriate class of curves, the problem *is constrained* by several required properties of visual interpolation. These properties were partially identified by Ullman (1976) as axioms, and more completely by Knuth (1979). Unfortunately, the latter set of proposed axioms is not consistent. Knuth, given the choice
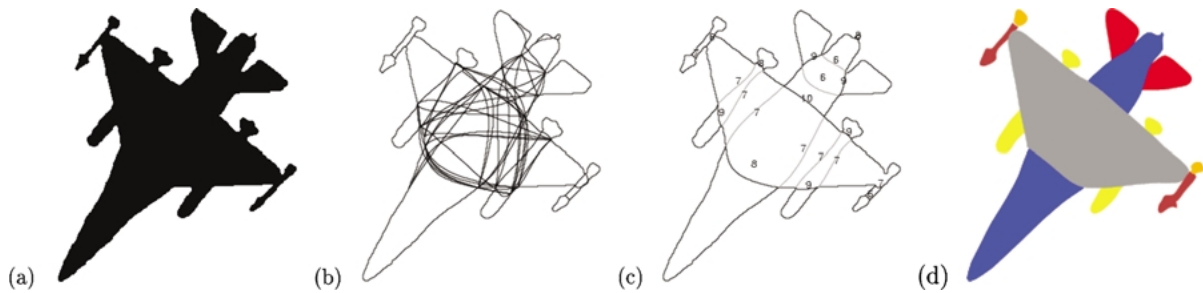
Figure 16.   This figure from (Siddiqi and Kimia, 1995) illustrates how stable partitioning can arise from disambiguating competing part-curve hypotheses. (a) original shape; (b) all part-curve hypotheses; (c) disambiguation using the saliency of the part-curve; (d) partitioning results. The Euler Spiral provides a better break curve and a better saliency measure (Dhandapani and Kimia, 2002).

between locality and extensibility, to make this set consistent, reluctantly drops extensibility. This solution violates roundedness. On the other hand, in this paper we examine the implications of retaining extensibility and dropping locality instead. This allows us to maintain roundedness, i.e., circular interpolations of point tangent pairs that are indeed on a circle. This in turn leads to an energy functional which penalizes curvature variation, but not curvature proper. The solution yields interpolations which are segments of the Euler Spiral, i.e., curves where curvature varies linearly with arclength. The rest of the paper deals with the derivation of analytic formulas for computing this curve using a biarc approximation which can then be refined to obtain the Euler spiral by solving a nonlinear system of two equations in two unknowns involving Fresnel Integrals.

The practical advantages of using an Euler spiral interpolation are: (i) fast and reliable completion curve computation; (ii) natural and intuitive completion curves; (iii) robustness to changes in the extent of occlusion: extensibility ensures that as a portion of the occluded contour modeled by an Euler spiral is revealed the interpolation does not change. This property is not true of the Ullman's biarc or our biarcs, nor of the scale-invariant elastica (regular elastica are extensible but change with scale); (iv) the Euler Spiral interpolates over a complete range and combinations of boundary data; (v) the internal parameters of the interpolant are geometrically meaningful and thus can be used as an indicator to dis-ambiguate edges in perceptual grouping, as suggested in (Guy and Medioni, 1992; Parent and Zucker, 1989; Sha'ashua and Ullman, 1988; Williams and Jacobs, 1995). Thus, it provides a suitable solution to the gap completion and boundary modeling problems as used in the context of perceptual grouping of edge maps, partitioning visual form, and filling-in of occluded objects among others.

Appendix A: Algorithm

We now describe the algorithms in pseudocode format for computing the parameters of the biarc, which has minimum total curvature derivative variation, and for computing the parameters of the Euler Spiral. Let (x_0, y_0, θ_0) and (x_2, y_2, θ_2) denote the initial and final coordinate-tangent angle pairs. The biarc algorithm returns K_1, L_1, K_2, L_2, the curvature and length of each arc as well as the total curvature variation E. The Euler Spiral algorithm returns the initial and final curvature K_0, K_2, the length L, the rate of change of curvature γ, and the total curvature derivative variation E.
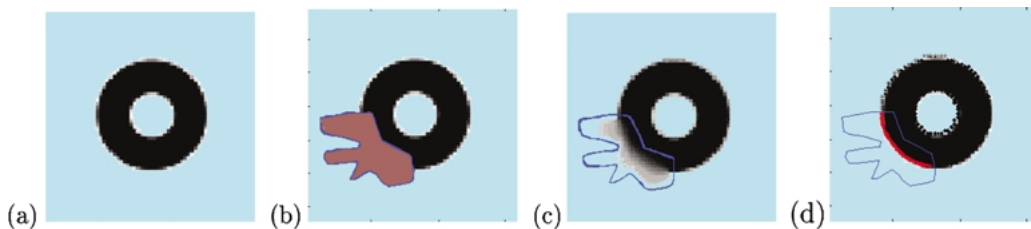

Figure 17.   (a) The original image, (b) The gap (in brown), (c) Inpainting using a conventional diffusion based technique, and (d) Inpainting using the Euler Spiral (in red) as the completion contour of the occluded object.

A.1. Pseudocode for Biarc Implementation

COMPUTEBIARCSOLUTION($x_0, y_0, x_2, y_2, \theta_0, \theta_2$)

```
1
2    L ← √((x₁ − x₀)² + (y₁ − y₀)²)
3    ψ ← AngleOfVector(x₂ − x₀, y₂ − y₀)
4    smallAngle ← 0.001
5    smallCurvature ← 0.001
6    biarc_flag ← 0
7    L₁ ← −10
8    L₂ ← −10
9    if (ψ − ((θ₂+θ₀)/2) mod π = 0)
10     then if ψ − θ₀ = 0
11        then
12               κ₁ ← 0
13               κ₂ ← κ₁
14               L₁ ← L/2
15               L₂ ← L₁
16
17        else
18               κ₁ ← (−2/L) sin((θ₂−θ₀)/2)
19               κ₂ ← κ₁
20               L₁ ← |θ₀L sin((π/2−θ₀)/sin(2*θ₀))|
21               L₂ ← L₁
22
23        θ_join ← θ₂
24        estimate_K ← κ₁
25        estimate_L ← L₁ + L₂
26
27     else
28        biarc_flag ← 1
29        κ₁ ← −(4/L) sin((3θ₀+θ₂)/4 − ψ) cos((θ₂−θ₀)/4)
30        κ₂ ← (4/L) sin((θ₀+3θ₂)/4 − ψ) cos((θ₂−θ₀)/4)
31        θ_join ← ComputeJoinTheta
32               (x₀, y₀, θ₀, x₂, y₂, θ₂, κ₁, κ₂)
33        if κ₁ == 0
34          then L₁ ← L (sin((θ₂+θ₀)/2−ψ))/(sin((θ₀−θ₂)/2))
35
36          else
37               L₁ ← ComputeArclength(θ₀, θ_join, κ₁)
38
39        if κ₂ == 0
40          then L₂ ← L sin((θ₂+θ₀)/2−ψ)/sin((θ₀−θ₂)/2)
41
42          else
43               L₂ ← ComputeArclength(θ_join, θ₂, κ₂)
44
45        κ₃ ← (4/L) cos((3θ₀+θ₂)/4 − ψ) sin((θ₂−θ₀)/4)
46        κ₄ ← (4/L) cos((θ₀+3θ₂)/4 − ψ) sin((θ₂−θ₀)/4)
47        if (κ₃ == 0) and (κ₄ == 0)
48          then Both curvatures are 0—e-approximations
49               needed
50          else
51               if (κ₃ ≠ κ₄)
52                 then
53                      θ_join ← ComputeJoinTheta
54                             (x₀, y₀, θ₀, x₂, y₂, θ₂, κ₃, κ₄)
55                      if κ₃ == 0
56                        then
57                             L₃ ← L sin((θ₂+θ₀)/2−ψ)/sin((θ₂−θ₀)/2)
58
59                        else
60                             L₃ ← ComputeArclength
61                                    (θ₀, θ_join, κ₃)
62
63                      if κ₄ == 0
64                        then
65                             L₄ ← L sin((θ₂+θ₀)/2−ψ)/sin((θ₀−θ₂)/2)
66
67                        else
68                             L₄ ← ComputeArclength
69                                    (θ_join, θ₂, κ₄)
70
71
72
73        E1 ← (κ₂ − κ₁)(κ₂ − κ₁)
74        E2 ← (κ₃ − κ₄)(κ₃ − κ₄)
75        estimate_L, estimate_K to be computed according
76        to correct criteria for choosing one of the two solutions
77        if L1 + L2 < L3 + L4
78          then
79               estimate_L ← L1 + L2
80               estimate_K ← κ₁
81          else
82               estimate_L ← L3 + L4
83               estimate_K ← κ₃
84        return estimate_K, estimate_L
85
```

ANGLEOFVECTOR(X, Y)

```
1
2    val_angle = arctan₂ (Y/X)
3    if val_angle < 0
4      then
5           val_angle ← (val_angle + 2π)
6
7    return val_angle
```

COMPUTEJOINTHETA($x_0, y_0, \theta_0, x_2, y_2, \theta_2, \kappa_1, \kappa_2$)

```
1    sin(θ_Join) ← (κ₁κ₂(x₂−x₀)+κ₂ sin(θ₀)−κ₁ sin(θ₂))/(κ₂−κ₁)
2    cos(θ_Join) ← (−κ₁κ₂(y₂−y₀)+κ₂ cos(θ₀)−κ₁ cos(θ₂))/(κ₂−κ₁)
3    θ_Join ← AngleOfVector(sin(θ_Join), cos(θ_Join))
4    return θ_Join
```

COMPUTEARCLENGTH(θ_0, θ_1, k)

```
1    numerator ← θ₁ − θ₀
2    if (k < 0) and ((θ₁ − θ₀) > 0)
3      then numerator ← (numerator − 2π)
4
5      else if (k > 0) and ((θ₁ − θ₀) < 0)
6           then numerator ← (numerator + 2π)
7
8    return numerator/k
9
```

A.2. Pseudocode for the Euler spiral

SOLVEEULER($x_0, y_0, \theta_0, x_2, y_2, \theta_2, iter_{num}$)
1 $estK_{init}, estL_{init} \leftarrow ComputeInitialEstimates$
2                     $(x_0, y_0, \theta_0, x_2, y_2, \theta_2)$
3 $\kappa_{fin}, L_{fin} \leftarrow SolveIteratively$
4                     $(x_0, y_0, \theta_0, x_2, y_2, \theta_2, estK_{init}, estL_{init}, iter_{num})$
5 $\gamma \leftarrow 2\frac{\theta_2-\theta_0-(\kappa_{fin}L_{fin})}{L_{fin},2}$
6 **return** $\kappa_{fin}, L_{fin}, \gamma$

COMPUTEINITIALESTIMATES($x_0, y_0, \theta_0, x_2, y_2, \theta_2$)
1 $estK_{init}, estL_{init} \leftarrow ComputeBiarcSolution$
2                     $(x_0, y_0, \theta_0, x_2, y_2, \theta_2)$
3 **return** $estK_{init}, estL_{init}$
4

SOLVEITERATIVELY($x_0, y_0, \theta_0, x_1, y_1, \theta_2, estK_{init}, estL_{init}, iter_{num}$)
1   $error \leftarrow computeError$
2               $(x_0, y_0, \theta_0, x_1, y_1, \theta_2, estK_{init}, estL_{init})$
3   $prevError \leftarrow 1000$
4   $errorStep \leftarrow 0.1$
5   $epsilon \leftarrow 0.00001$
6   $epsilonError \leftarrow 0.1$
7   $curEstK \leftarrow estK_{init}$
8   $curEstL \leftarrow estL_{init}$
9   **for** $i \leftarrow 0$ **to** $iter_{num}$
10   **do**
11   **if** ($error < epsilon$)**or**($i == iter_{num} - 1$)
12   **then**
13   **return** $curEstL, curEstK$
14
15   **else**
16              $error_0 \leftarrow computerror$
17   $(x_0, y_0, \theta_0, x_1, y_1, \theta_2, (curEstK + errorStep), curEstL)$
18              $error_1 \leftarrow computeError$
19   $(x_0, y_0, \theta_0, x_1, y_1, \theta_2, (curEstK - errorStep), curEstL)$
20              $error_2 \leftarrow computeError$
21   $(x_0, y_0, \theta_0, x_1, y_1, \theta_2, curEstK, (curEstL + errorStep))$
22   **if** $estL > errorStep$
23   **then**
24                      $estL \leftarrow (curEstL - errorStep)$
25                      $error_3 \leftarrow computeError$
26                          $(x_0, y_0, \theta_0, x_1, y_1, \theta_2, curEstK, estL)$
27              $error \leftarrow min(error_0, error_1, error_2, error_3)$
28   **if** $error >= prevError$
29   **then** $errorStep \leftarrow \frac{errorStep}{2}$
30
31   **else if** $error == error_0$
32   **then**
33                       $curEstK \leftarrow (curEstK + errorStep)$
34
35   **else if** $error == error_1$
36   **then**
37                       $curEstK \leftarrow (curEstK - errorStep)$
38
39   **else if** $error == error_2$
40   **then**
41                       $curEstL \leftarrow (curEstL + errorStep)$
42
43   **else if** $curEstL > errorStep$
44   **then**
45                       $curEstL \leftarrow (curEstL - errorStep)$
46
47              $prevError \leftarrow error$

COMPUTEERROR($x_0, y_0, \theta_0, x_2, y_2, \theta_2, \kappa, L$)
1 $\gamma \leftarrow 2\frac{\theta_2-\theta_0-(\kappa L)}{L^2}$
2 $X, Y \leftarrow EulerSpiralEndPoint(x_0, y_0, \theta_0, \kappa, \gamma, L)$
3 $error = \sqrt{(X - x_2)^2 + (Y - y_2)^2}$
4 **return** $error$

EULERSPIRALENDPOINT($a, b, \theta, \kappa, \gamma, s$)
1   $\epsilon = 0.00000001$
2   **if** $(\gamma > 0 and \gamma < \epsilon)or(\gamma < 0 and \gamma > \epsilon)$
3   **then**
4       $\gamma \leftarrow 0$
5   **if** $\gamma > 0$
6   **then**
7              $first \leftarrow fresnel(\frac{\kappa+(\gamma s)}{\sqrt{(\pi\gamma)}})$
8              $second \leftarrow fresnel(\frac{\kappa}{\sqrt{(\pi\gamma)}})$
9              $A \leftarrow first[0] - second[0]$
10             $B \leftarrow first[1] - second[1]$
11             $cosTerm \leftarrow \cos(\theta - \frac{\kappa^2}{2\gamma})$
12             $sinTerm \leftarrow \sin(\theta - \frac{\kappa^2}{2\gamma})$
13             $constTerm = \sqrt{(\frac{\pi}{\gamma})}$
14     $X \leftarrow a + (constTerm)(cosTermA - sinTermB)$
15     $Y \leftarrow b + (constTerm) * (sinTermA + cosTermB)$
16   **if** $\gamma < 0$
17   **then**
18                    $first \leftarrow fresnel(\frac{-\kappa+(-\gamma s)}{\sqrt{(-\pi\gamma)}})$
19                    $second \leftarrow fresnel(\frac{-\kappa}{\sqrt{(-\pi\gamma)}})$
20                    $A \leftarrow first[0] - second[0]$
21                    $B \leftarrow -(first[1] - second[1])$
22                    $constTerm \leftarrow (\sqrt{\frac{\pi}{-\gamma}})$
23                    $cosTerm = \cos(\theta - (\kappa^2)/(2\gamma))$
24                    $sinTerm = \sin(\theta - (\kappa^2)/(2\gamma))$
25        $X \leftarrow a + (constTerm)(cosTermA - sinTermB)$
26        $Y \leftarrow b + (constTerm)(sinTermA + cosTermB)$
27
28 **if** $\gamma = 0$
29 **then**
30   **if** $\kappa = 0$
31   **then**
32            $X \leftarrow a + scos(\theta)$
33            $Y \leftarrow b + ssin(\theta)$
34
35   **else** $constTerm \leftarrow \frac{1.0}{kappa}$
36            $X \leftarrow a + (constTerm)(\sin(\kappa s + \theta) - \sin(\theta))$
37            $Y \leftarrow b + (-constTerm)(\cos(\kappa s + \theta) - \cos(\theta))$
38   **return** X, Y

Acknowledgments

Notes

1. The main reason for using $(0, 2)$ is to facilitate the use of an intermediate point (index 1).
2. The notation (x_0, y_0, θ_0) denotes that the interpolation passes through (x_0, y_0) at tangent angle θ_0.
3. According to Knuth, prior attempts at laying a scientific foundation for calligraphy and mathematical typography, e.g., those of Feliciano (1460), Pacivoli (1509), Torriello (1517), Palatino (1574), Tory (1579) and Maxon (1676), relied on "rigid ruler and compass" methods and, were aesthetic failures, "deprived of calligraphic grace".
4. It is curious that, in actual applications of this curve completion solution, the resulting curve does not, unlike Renaissance geometers, describe the boundary of a symbol; rather, it describes the "central curve" of the symbol and, as such, allows the shape of the pen to vary. This is precisely a description of shape as the geometry of the medial axis curve as well as the radial or dynamic changes as a point moves along this axis (Knuth, 1979).
5. It should also be noted that Grossberg and Mingolla (1985) propose a cooperative-competitive framework consisting of iterative nonlinear convolutions to complete illusory contours, among other tasks.
6. The curvature of an elastic curve meeting these end conditions (but with free length) satisfies (Birkhoff and Boor, 1965)

$$\kappa_{ss} + \frac{1}{2}\kappa^3 = 0.$$

7. If we posit κ_0 and L as the free parameters, γ can be eliminated by $\gamma = 2\frac{(\theta_1 - \theta_0) - \kappa_0 L}{L^2}$, in Eq. (3), leading to two equations and two unknowns. However, numerical experience with these geometric interpolants shows that another set of free parameters, namely, κ_0 and κ_2 (initial and final curvatures), is better suited to the recovery of the Euler spiral. In other words, we use an alternate, more symmetric, yet equivalent, description of each Euler Spiral segment in terms (x_0, y_0, θ_0) and $(\kappa_0, \kappa_2, \gamma)$
8. We use subscript two to allow for the intermediate point (x_1, y_1, θ_1) which joins two biarcs.
9. It is instructive to consider the limiting case of the second solution as $\theta_2 \to \theta_0$; let $\theta_2 = \theta_0 + \epsilon$ where ϵ is a small number. The second solution implies very small and close curvatures, corresponding to a biarc consisting of very large circles. In the limit, the biarc consists of two infinite length line segments joining at infinity. Note also that by taking ϵ arbitrarily small, the second solution can be made to have smaller $|\kappa_2 - \kappa_1|$ but at the expense of arbitrarily enlarging its length. Since the Euler spiral corresponding to one extreme biarc may be "better" than another, even when the corresponding biarcs hold the opposite relationship, we consider both extremal solution to generate the Euler spiral.

References

Abramowitz, M. and Stegun, I.A. (eds.) 1972. *Handbook of Mathematical Functions with Formulas, Graphics, and Mathematical Tables*. National Bureau of Standards, New York.

Ahlberg, J., Nilson, E., and Walsh, J. 1967. *The Theory of Splines and their applications*. New York, Academic Press.

Baldwin, A. 1996. Teardrop & clothoid loops. www.demon.co.uk/arvis/wwg/tech/phtd.html.

Birkhoff, G. and Boor, C.D. 1965. Piecewise polynomial interpolation and approximation. *Approximations of Functions*.

Brady, M. and Grimson, W. 1980. Shape encoding and subjective contours. In *Proc. 1st Annual National Conf. on Artif. Intel.*, pp. 15–17.

Bryant, R. and Griffiths, P. 1986. Reduction for constrained variational problems and $\int \frac{\kappa^2}{2} ds$. *American Journal of Mathematics*, 108:525–570.

Cesaro, E. 1886. Les lignes barycentriques. *Nouvelles annales de mathematiques*, 3(5):511–520.

Cornu, A. 1874. Methode nouvelle pour la discussion des problèmes de diffraction. *Journal physique théorique et appliquée*.

Dhandapani, R. and Kimia, B.B. Role of scale in partitioning shape. In *Proceedings of the IEEE International Conference on Image Processing*, Rochester, New York, IEEE Computer Society Press (Accepted).

Euler, L. 1744. *Methodus inveniendi lineas curvas maximi minimive proprietate gaudentes*. Lausanne.

Euler's integrals and Euler's spiral. 1918. *American Math Monthly*, Vol. 25(8).

Farin, G.E. 1996. *Curves and Surfaces for Computer-Aided Geometric Design: A Practical Guide (Computer Science and Scientific Computing Series)*, 4th ed. Academic Press.

Grossberg, S. and Mingolla, E. 1985. Neural dynamics of form perception: Boundary completion, illusory figures, and neon color spreading. *Psychological Review*, 92(2):173–211.

Guy, G. and Medioni, G. Perceptual grouping using global saliency-enhancing operators. In *International Conference on Pattern Recognition*, The Hague, Netherlands, August 30–September 3, 1992. Computer Society Press, pp. I:99–103.

Herault, L. and Horaud, R. 1993. Figure-ground discrimination: A combinatorial approach. *PAMI*, 15(9):899–914.

Higgins, A. 1921. *The Transition Spiral and its Introduction to Railway Curves*. Constable, London.

Hoffman, D.D. and Richards, W.A. 1985. Parts of recognition. *Cognition*, 18:65–96.

Horn, B.K.P. 1983. The curve of least energy. *ACM Trans. Math. Softw.*, 9(4):442–460.

Johannes, M.S., Sebastian, T.B., Tek, H., and Kimia, B.B. 2001. Perceptual organization as object recognition divided by two. In *Workshop on Perceptual Organization in Computer Vision*, pp. 41–46.

Kanizsa, G. 1979. *Organization in Vision: Essays on Gestalt Perception*. Praeger.

Knuth, D.E. 1979. Mathematical typography. *Bulletin (new series) of the American mathematical Society*, 1(2):337–372.

Kurtz, C. 1945. *Track and Turnout Engineering*. Simmons-Boardman Publishing Corporation, New York.

Leonard, I. 1988. More on Fresnel integrals. *American Mathematical Monthly*, 95:431–433.

Love, A. 1927. *A Treatise on the Mathematical Theory of Elasticity*, 4th ed. Cambridge University Press, Cambridge.

Mumford, D. 1994. Elastica and computer vision. In *Algebraic Geometry and Its Applications*, Springer-Verlag, pp. 491–506.

Nitzberg, M., Mumford, D., and Shiota, T. 1993. *Filtering, Segmentation and Depth*. Springer-Verlag.

Onn, R. and Bruckstein, A. 1990. Integrability disambiguates surface recovery in two-image photometric stereo. *International Journal of Computer Vision*, 5:1:105–113.

Parent, P. and Zucker, S.W. 1989. Trace inference, curvature consistency and curve detection. *PAMI*, 11(8):823–839.

Press, W., Flannery, B., Teukolsky, S., and Vetterling, W. 1993. *Numerical Recipes in C: The Art of Scientific Computing*, 2nd ed., Fresnel Integrals, Cosine and Sine Integrals. Cambridge University Press, Cambridge, England.

Rutkowski, W.S. 1979. Shape completion. *Computer Graphics and Image Processing*, 9:89–101.

Sarkar, S. and Boyer, K. 1992. Perceptual organization using Bayesian networks. In *CVPR92*, pp. 251–256.

Sha'ashua, A. and Ullman, S. 1988. Structural saliency: The detection of globally salient structures using a locally connected network. In *Second International Conference on Computer Vision* (Tampa,, FL, December 5–8, 1988), Washington, DC, IEEE Computer Society Press.

Sharon, E., Brandt, A., and Basri, R. Completion energies and scale. *IEEE Transactions on Pattern Analysis and Machine Intelligence* 22(10):1117–1131, October 2000.

Siddiqi, K. and Kimia, B.B. 1995. Parts of visual form: Computational aspects. *PAMI*, 17(3):239–251.

Sokolnikoff, J. 1956. *Mathematical Theory of Elasticity*. New York.

Spanier, J. and Oldham, K. 1987. *An Atlas of Functions*. Hemisphere, Washington, DC.

Talbot, A.N. 1927. *The Railway Transition Spiral*, 6th ed. McGraw-Hill Book Company, Inc., New York and London.

Ullman, S. 1976. Filling-in the gaps: The shape of subjective contours and a model for their generation, 25:1–6.

Weiss, I. 1988. 3D shape representation by contours. *Computer Vision, Graphics, and Image Processing*, 41:80–100.

Weisstein, E.W. 1998. French curve. www.astro.virginia.edu/~eww6n/math/FrenchCurve.html.

Williams, L. and Jacobs, D. 1997. Local parallel computation of stochastic completion fields. *Neural Computation*, 9(4):837–858.

Williams, L. and Thornber, K. 1998. A comparison of measures for detecting natural shapes in cluttered backgrounds. *ECCV98*, 1407(2):432–448.

Williams, L. and Thornber, K. 1999. A comparison of measures for detecting natural shapes in cluttered backgrounds. *IJCV*, 34(2/3):81–96.

Williams, L.R. and Jacobs, D.W. 1995. Stochastic completion fields: A neural model of illusory contour shape and salience. In *Proceedings of the Fifth International Conference on Computer Vision*, Boston, Massachusetts, IEEE Computer Society Press, pp. 408–415.